https://doi.org/10.5194/egusphere-2023-1694
Preprint. Discussion started: 1 August 2023

Coupled atmosphere-ocean simulations of contemporary and future South Pacific tropical cyclones

Jonny Williams[1], Erik Behrens[1], Olaf Morgenstern[1], Peter B. Gibson[1], and João C. M. Teixeira[2]

[1]NIWA, 301 Evans Bay Parade, Wellington, 6021, New Zealand
[2]Met Office, Fitzroy Road, EX1 3PB, Exeter, UK

Correspondence: Jonny Williams (jonny.williams@niwa.co.nz)

Abstract. Tropical cyclones – TCs – affecting the South Pacific region are studied using coupled atmosphere-ocean earth system models and (offline) storm tracking software which tracks the position of simulated pressure lows through time. The models used are the United Kingdom Earth System Model, version 1 – UKESM1 – and the related New Zealand Earth System Model, the NZESM. The model pair considered here differ only in their treatment of the ocean and the NZESM has a nominal resolution of 0.2° in the region surrounding New Zealand and 1° elsewhere; UKESM1 has a a uniform 1° resolution everywhere. After validating the storm tracking algorithm against the track of cyclone Giselle from 1968 and cyclone Gabrielle from 2023 we use the Saffir-Simpson scale to split the tracked systems into categories based on their severity. For systems formed in the vicinity of New Zealand (and globally) the overall number is overestimated but stronger (category 2 and 3) storms are underestimated. We also see a general decrease in the total number of storms as radiative forcing, $\mathcal{F}$, increases although there is some evidence of a small increase at extreme levels of warming. In the metrics studied here we find no difference between the ensembles of UKESM1 and NZESM simulations and going forward use the UKESM1, which has larger available ensembles. The power dissipation index, PDI, gives a first order measure of TC strength and we find that the average PDI per storm increases with $\mathcal{F}$ by up to 26% under a 'fossil-fuelled development' scenario. Although the physical mechanisms behind the increase in average PDI with $\mathcal{F}$ are relatively simple to understand, those governing the frequency of occurrence are not. In the results shown here, vertical wind shear increases with $\mathcal{F}$ which tends to reduce TC numbers but the effect of the tropospheric relative humidity is much less clear. The increase in the area of the tropics bounded by the 26.5° isotherm should, on its own, increase the number of TCs, in opposition to the general behaviour observed, except perhaps at extreme levels of future warming.

1 Introduction

In February 2023, ex-tropical cyclone Gabrielle impacted several countries in the South Pacific and caused the largest financial fallout of any South Pacific tropical cyclone on record, as well as causing 11 fatalities. Gabrielle was a category 3 tropical cyclone and is precisely the type of system which society would like to have a better understanding of in a changing climate.

A further example of an ex-tropical cyclone impacting New Zealand came in April 1968 in which cyclone Giselle caused the sinking of the passenger vessel Wahine with the loss of over 50 lives.

https://doi.org/10.5194/egusphere-2023-1694
Preprint. Discussion started: 1 August 2023

Although these two particular storms are far from unique in their physical attributes, they occupy a particularly visceral location in the public psyche of New Zealanders and are used in this study as benchmarks to validate cyclone tracking software.

Understanding how TCs may change in the future has enormous ramifications. For example, some authors predict that climate change may *double* the economic impact of TCs by 2100 (Mendelsohn et al., 2012). Changes to populations, poverty levels and the ability of affected governance structures to deal with TC impacts are also of paramount importance(Noy, 2016; Peduzzi et al., 2012).

All these issues notwithstanding, without a way to explicitly track low pressure systems through time we can't even begin to quantify TCs and their impacts as the climate changes.

As far as mean-sea-level pressure is concerned, global climate models typically produce gridded data with a resolution of the order of 1° which is enough to detect and follow TCs around. Various algorithms and software schemes are available.

The scheme of Hodges et al., `TRACK` (Hodges, 1994, 1995, 1999) has been widely used in the literature but is not open-source, although it does track spatial features in 850hPa vorticity and thus has the advantage of being able to find storms early in their lifetime.

In this study we use the open source `stormTracking` package [1], which identifies pressure extrema and their paths through time. This is an adapted version of an ocean eddy tracking code described in detail in (Chelton et al., 2011) and a full description of how it works is included in Appendix B. The `tempestExtremes` software described in (Ullrich et al., 2021) is another open-source package which uses sea-level-pressure data to track storms and a comparison between the results of this package with `stormTracking` is given below. We also provide a comparison of the ability of the 20CR and ERA5 reanalyses to follow the observed track of cyclone Giselle and subsequently use ERA5 because of its higher resolution and its improved ability to to capture deep lows.

The study of Roberts et al. (Roberts et al., 2020a) compares the results of `TRACK` and `tempestExtremes` using simulations from the High Resolution Model Intercomparison Project, HighResMIP (Haarsma et al., 2016) out to 2050. They find an overall decrease in the number of Southern Hemisphere TCs in the Indian Ocean but results for the Northern Hemisphere and indeed other Southern Hemisphere ocean basins are unclear. They also note – and the present study agrees – that the most damaging TCs are set to increase in their damage potential; indeed this – along with a general uncertainty concerning TC occurrence frequency – is the broad consensus of the research community at the time of writing. They also find that refining the resolution of the model used has an overall positive effect on its ability to simulate important TC properties. In a companion paper (Roberts et al., 2020b), the same two tracking algorithms are used on a related ensemble but for the historical period covering 1950-2014 and – notably for this study – find that the frequencies of the highest category TCs are underestimated.

Some previous studies have found that Southern hemisphere tropical cyclone – TC – frequency is set to reduce as the climate warms yet some have found the opposite (see (Chand et al., 2022) for a recent review). In contrast, the strength of the 'remaining' TCs is – more robustly – projected to increase (Knutson et al., 2010; Chand et al., 2022; Emanuel, 2005). The number of TCs is also highly dependent on the ocean basin considered with the South Atlantic for example producing few-to-none (Pezza and Simmonds, 2005). Our results broadly agree these findings from previous studies.

[1] https://github.com/ecjoliver/stormTracking/

https://doi.org/10.5194/egusphere-2023-1694
Preprint. Discussion started: 1 August 2023

We firstly compare simulated, historical tropical cyclone climatologies in the New Zealand region and globally against reanalysis data and then perform the same analysis for the whole Southern Hemisphere.

We then move on to assessing potential future changes to storms at the end of the 21st century using various different Shared Socioeconomic Pathways, allowing for quantification of possible future greenhouse gas emissions (Riahi et al., 2017; Meinshausen et al., 2020). Our results show some evidence for a reduction in the number of Southern Hemisphere TCs expected as the climate warms and a more robust expectation for increased TC strength.

TC formation (cyclogenesis) involves a highly complex set of inter-related physical criteria on sea surface temperature (SST), humidity and wind shear which goes some way to explain why the future frequency of TCs is difficult to predict and all three of these effects are considered in this work. To first order, wind shear changes tend to reduce the number of TCs, SST tends to increases it and the effect of relative humidity is uncertain. We show some preliminary evidence that in extreme future warming scenarios that the effect of increasing SST *may* overwhelm the factors tending to reduce TC numbers although.

Regarding the future strength of TCs, we quantify how we may expect power dissipation per TC – and hence damage inflicted – to increase based on future scenarios of climate change and although the precise magnitude of this is uncertain, the direction is robust, in agreement with the current literature.

2 Comparing tracking algorithms

To better understand the uncertainty associated with the use of different tracking algorithms, we start by comparing the outputs of the `stormTracking` and `tempestExtremes` using ERA5 data from 1989-2008 as ground truth, Figure 1. The minimum storm duration considered is 54 hours – the `tempestExtremes` default value – and the input data for `stormTracking` is regridded to a resolution of 2° before the processing algorithm is applied. The reason for this is that the default input dataset to `stormTracking` is the 20CR reanalysis which has a resolution of 2°. Only storms which have their genesis in -20° < latitude < 0° and 132.7° < longitude < 216.3° are considered. The longitude bounds here are those of the high-resolution ocean region in the NZESM, which is described in §4 and in (Behrens et al., 2020).

The agreement between the two results in 1 shows that the two different algorithms are in good agreement with one another, particularly in the number and spatial distribution of genesis sites. Overall, the `stormTracking` results in Figure 1 are more sparse further away from the genesis sites compared to `tempestExtremes`. This is likely due to the regridding which is applied to the input data for this algorithm which removes a substantial amount of the spatial information present in the raw data. This is quantified by the number of storms reaching south of -60°, $N_{\lambda<-60}$, which is 6 in Figure 1(a) and 11 in Figure 1(b). However, the agreement is striking and – along with the validation for TCs Giselle and Gabrielle below – gives confidence that the `stormTracking` software is fit for purpose and for the remainder of this study `stormTracking` is used exclusively.

https://doi.org/10.5194/egusphere-2023-1694
Preprint. Discussion started: 1 August 2023

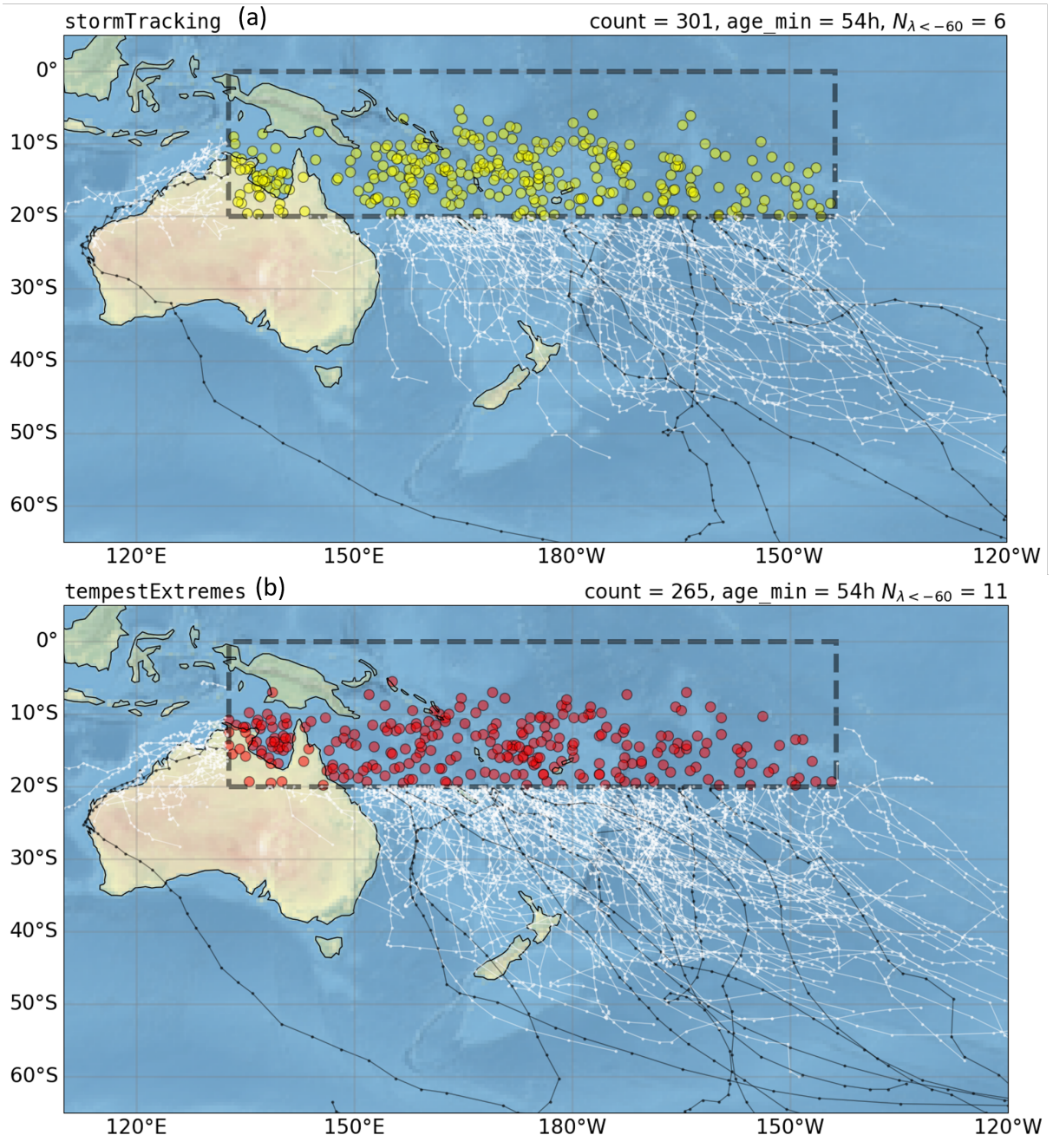

Figure 1. Tropical cyclone climatologies for the `stormTracking` – (a) – and `tempestExtremes` – (b) – software packages. The input data is 6-hourly mean-sea-level pressure for 1989-2008 from the ERA5 reanalysis. Only storms with duration 54h or more are considered and the black tracks are for storms which reach south of -60°, the sum of which is denoted $N_{\lambda<-60}$.

https://doi.org/10.5194/egusphere-2023-1694
Preprint. Discussion started: 1 August 2023

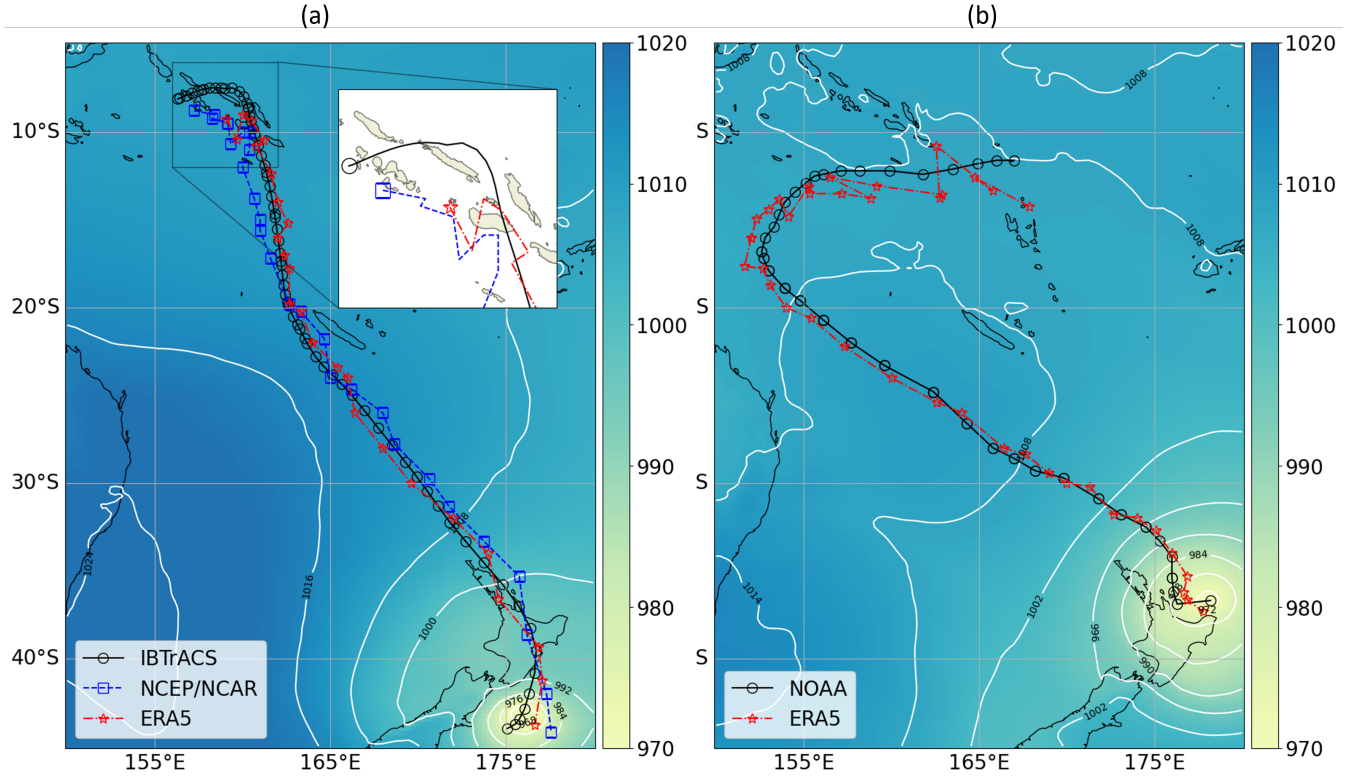

Figure 2. (a) Observed (Knapp et al., 2010) track from IBTrACS of cycle Giselle (○) which hit Wellington in April 1968 causing the Wahine disaster. All tracks show data from the beginning of the respective datasets and are terminated at 19680410T0600Z which is also the date of the background pressure map, also from ERA5. The inset zooms in on the cyclogenesis region. (b) Observed track from NOAA of cycle Gabrielle (○) which hit New Zealand in February 2023. Both tracks show data from the beginning of the respective datasets and are terminated at 20230214T0000Z which is also the date of the background pressure map, also from ERA5. NOAA data for Gabrielle is available at https://www.ssd.noaa.gov/PS/TROP/DATA/ATCF/JTWC/bsh122023.dat.

3 Validation of storm tracking software

We now move on to validating the chosen algorithm on the two specific TCs mentioned in the introduction; Giselle from 1968 and Gabrielle from 2023.

3.1 Giselle, April 1968

Cyclone Giselle struck New Zealand and caused the sinking of the passenger ferry Wahine in April 1968. Giselle was an ex-tropical cyclone and its path over the preceding 8 days is shown in Figure 2.

Figure 2 shows the track of cyclone Giselle from two perspectives. Firstly from the IBTrACS database (Knapp et al., 2010) and secondly by processing sea-level pressure data from the 20CR (Compo et al.) and ERA5 (Hersbach et al., 2020) reanalyses.

https://doi.org/10.5194/egusphere-2023-1694
Preprint. Discussion started: 1 August 2023

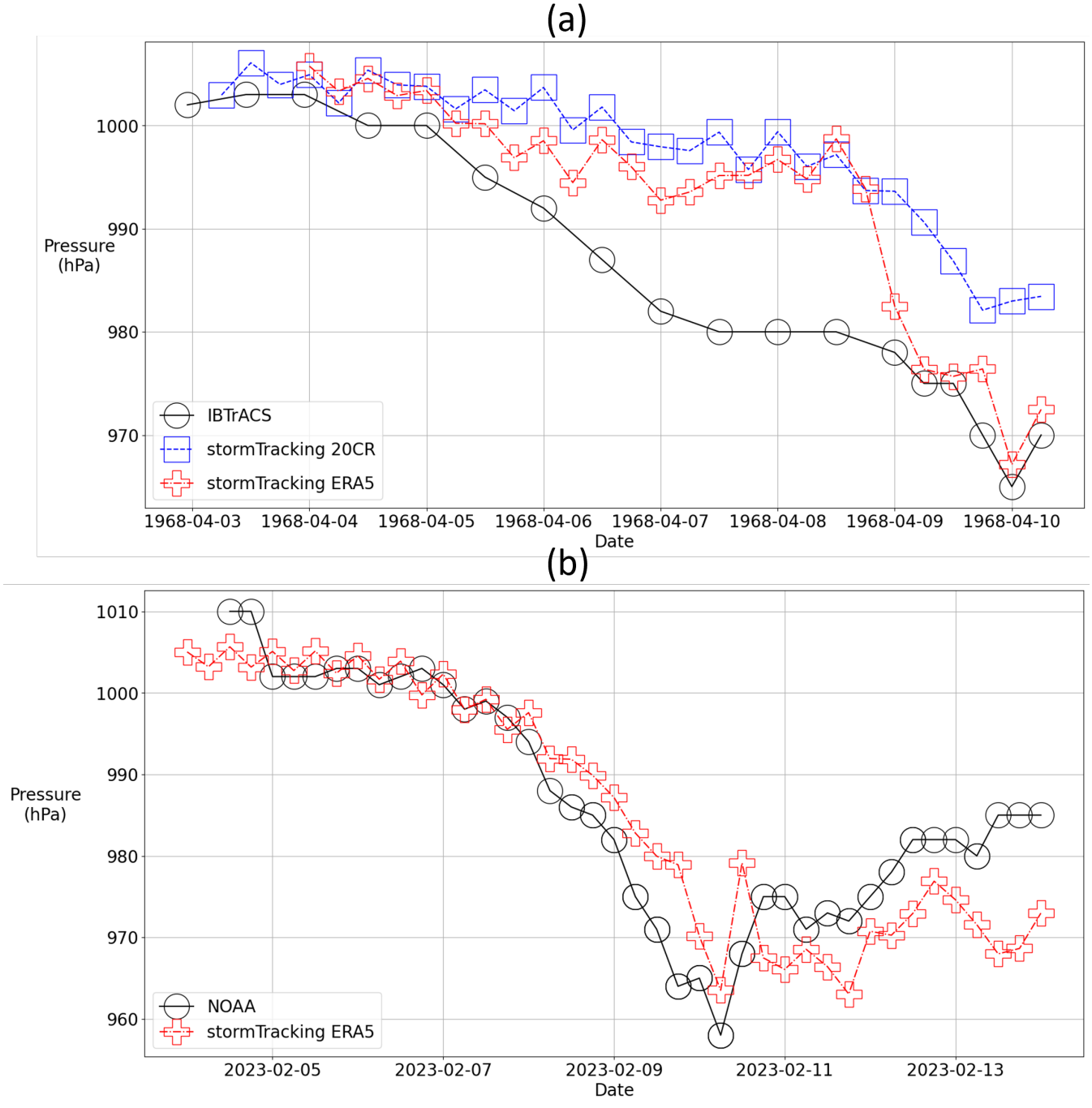

Figure 3. (a) Observed central pressure of storm Giselle from the IBTrACS database (Knapp et al., 2010) and the calculated values from the ERA5 (Hersbach et al., 2020) and 20CR (Compo et al.) reanalyses. All tracks show data from the beginning of the respective datasets and are terminated at 19680410T0600Z which is the date of the background pressure map in Figure 2. (b) Observed central pressure of storm Gabrielle from NOAA – see footnote in Figure 2 – and the calculated values from the ERA5 (Hersbach et al., 2020) reanalysis. All tracks show data from the beginning of the respective datasets and are terminated at 20230214T0000Z which is also the date of the background pressure map in Figure 2.

https://doi.org/10.5194/egusphere-2023-1694
Preprint. Discussion started: 1 August 2023

At first sight, it is perhaps not surprising that the 3 tracks shown in Figure 2(a) are so similar. They are, after all, representations of the same weather system. However the resolution of the 20CR reanalysis is $2° \times 2°$ and that of ERA5 is 8 times greater, $0.25° \times 0.25°$, i.e. 64 times the areal resolution of 20CR. However, the `stormTracking` package regrids all data to the same resolution as the 20CR reanalysis, that is, the software's default setting.

To better visualise the difference that this makes to the ability of the respective reanalyses to reproduce the physical characteristics of tropical cyclones, Figure 3 shows the magnitude of the central pressure for storm Giselle. The extreme low pressure around April 10th 1968 – ultimately the cause of the loss of life discussed above – is well captured by the ERA5 dataset but poorly by 20CR. Indeed, the observed precipitous drop in central pressure in from `18:00` on April 9th to `00:00` on April 10th is completely absent from 20CR. This is likely due to improved New Zealand-based observations in ERA5, such as upper-air soundings – e.g. (Tradowsky et al., 2018) – and four-dimensional variational data assimilation (Bell et al., 2021); indeed the 20CR reanalysis uses only surface data. For another comparison of these reanalyses, recent work has analysed both in terms of their Southern Annular Mode response (Morgenstern, 2021). An idea of the spatial scale of these systems can be seen in Figure 6 below.

3.2 Gabrielle, February 2023

During preparation of this manuscript – once Section §3.1 had been written – New Zealand and other neighbouring countries were hit by cyclone Gabrielle. Gabrielle was – by some measures – the most financially damaging event in New Zealand's history (Harrington et al., 2023), as well as causing the deaths of 11 people. Figures 2(b) and 3(b) show Gabrielle's track and central pressure respectively.

The track data in Figure 3 shows that the `stormTracking` software does not converge onto the observed track for a couple of days. This is not surprising however since the ERA5 data are regridded before applying the tracking algorithm. Once the tracks converge, again the agreement between the precisely observed locations and those re-analysed from the ERA5 data is excellent and the observed central pressures – Figure 3(b) – are closely followed.

As well as being a further check on the efficacy of the tracking algorithm used and providing a more recent example of a notably devastating system, it is interesting to note the 'noisier' contours in Figure 3(a) compared to 3(b). This is the case despite both sets of contours being taken from the same input dataset and illustrates the increased density of observations assimilated into the forcing model in the reanalysis in the intervening half-century.

4 Models used

We use results from UKESM1 (Sellar et al., 2019, 2020) and the NZESM (Behrens et al., 2020; Williams et al., 2023) and compare their results with reanalysis data from and ERA5 (Hersbach et al., 2020) all simulations are detailed in Table 3.

UKESM1 – United Kingdom Earth System Model – is a state-of-the-art, coupled earth system model – ESM – consisting of dynamic atmosphere, land-surface, ocean and sea ice models with the addition of biogeophysical and biogeochemical components (including an explicit troposphere-stratosphere chemistry scheme) and was a constituent model in CMIP6 ensemble.

https://doi.org/10.5194/egusphere-2023-1694
Preprint. Discussion started: 1 August 2023

These additional components of the model are what differentiates an 'Earth System' model from a 'physical' climate model such as the HadGEM3-GC3.1 model (Williams et al., 2018), which is the so-called 'physical core' of UKESM1. We use 16 members of UKESM1 historical ensemble and 5-member ensembles of each of the Shared Socio-economic Pathways (SSPs) in Table 1.

The NZESM is a closely-related sibling model of UKESM1 but contains a two-way nested, high-resolution (eddy permitting) ocean surrounding the New Zealand region from -60.17°S to -10.5°S and 132.70°E to 216.3°E at a nominal resolution of $\approx 0.2°$. This region is called the 'AGRIF' region for the rest of this work, where AGRIF stands for Adaptive Grid Refinement In Fortran (Debreu et al., 2008). The precise resolution depends on latitude and longitude and a more extensive treatment of the physics and physical oceanography of this model pair can be found elsewhere (Behrens et al., 2020, 2022). The NZESM also contains a change to the way that ozone photolysis is treated via the inclusion of a solar cycle dependence (Dennison et al., 2019). The atmospheric resolution of the models is $1.25° \times 1.875°$ and that of the global ocean is $\sim 1°$ but varies somewhat depending on latitude (Sellar et al., 2019).

Throughout this work we compare 'historical' results for 1989-2008 and future scenarios for 2080-2099. The forcings after 2015 – the end of the historical period for CMIP6 – are described in Table 1 and are described in detail elsewhere, e.g. (O'Neill et al., 2016; Van Vuuren et al., 2017; Fricko et al., 2017; Fujimori et al., 2017; Kriegler et al., 2017).

Additional historical simulations were carried out to test:

- The length of the spinup of the NZESM by starting in:
  - 1950, NZESM.
  - 1940 ($\times$ 2), NZESM2,3.
  - 1851, NZESM4. All UKESM historical ensemble members start in 1850, the extra year accounts for the first archived January 1st boundary conditions from the parent models.
- Hardware and compiler dependency.
  - The present authors used a Cray XC50 machine and the Intel Fortran compiler; UKESM1_NZ (UKESM1 simulations were run on a Cray XC40 machine using the native compiler).
- Solar-cycle dependence of ozone photolysis, NZESM_WITHOUT_PHOTOLYSIS_CHANGE.

5 Results

5.1 Cyclone occurrence frequency - comparison to ERA5

TC severity is often delineated using the Saffir-Simpson scale (Song et al., 2010) and we use the pressure bounds to define the different categories in Table 2.

https://doi.org/10.5194/egusphere-2023-1694
Preprint. Discussion started: 1 August 2023

SSP 'family'	Scenarios; $\mathcal{F}$ at 2100 [$\mathrm{W \cdot m^{-2}}$]	Description (overview in (O'Neill et al., 2016))
1	1.9 , 2.6	'Sustainability'(Van Vuuren et al., 2017)
2	4.5	'Middle of the road'(Fricko et al., 2017)
3	7.0	'Regional rivalry'(Fujimori et al., 2017)
5	8.5	'Fossil-fuelled development'(Kriegler et al., 2017)

Table 1. Shared socioeconomic pathways – SSPs – used in this work. The names used throughout this paper are formed by joining the SSP 'family' (1, 2, 3, 5) and the value of $\mathcal{F}$ (1.9, 2.6, 4.5, 7.0, 8.5), e.g. SSP2-4.5. $\mathcal{F}$ is the top of atmosphere radiative forcing at 2100 in $\mathrm{W \cdot m^{-2}}$.

Category	Pressure bounds
1	$980 < P$
2	$965 < P_{min} < 980$
3	$945 < P_{min} < 965$
4	$920 < P_{min} < 945$
5*	$P_{min} < 920$

Table 2. Category 1-3 definitions for the Saffir-Simpson scale. * None detected in any of the datasets examined in this work.

The scale goes up to category 5, however our results show no TCs in this category for any of the datasets considered and indeed too few category 4 ones to draw any conclusions from. This is of course not to say that these systems do not occur, simply that they do not show up in our reanalysed results. This is a known limitation of cyclone tracking algorithms, e.g. (Roberts et al., 2020b). Recent work has shown that a resolution of $\lessapprox 0.5^\circ$ gives improved representations of TCs in climate models (Cavicchia et al., 2023) and future work using this family of models to explicitly compare against the results presented here would be instructive.

Figures 4 shows the distribution of storms in categories 1 to 3 on the Saffir-Simpson scale as well as the total number, N, for the region considered in Figure 1. All data in Table 3 is shown. From here on the minimum age of systems considered is 72 hours, which is the default minimum in the `stormTracking` package. Figure 4(a) shows N and there is some evidence of a decrease as the forcing increases, although the data is noisy to say the least. Note also that the x-axis is also simply a 'count' of the number of models and although the forcing increased from left to right, there are more than 3 times the number of simulations with historical forcing than any of the SSPs.

The simulations universally overestimate N – Figure 4(a) – compared to ERA5 for the historical simulations by roughly 10-20%. However, given the myriad of approximations going into the tracking software and the regridding done before analysis, the results here are encouraging, particularly for this preliminary analysis. N_{cat1} is also overestimated and $N_{cat2,3}$ are underestimated. This tendency to 'lose' higher category systems is a known feature of `tempestExtremes` and the same likely applies to `stormTracking` too given the similarity of the two algorithms.

Figure 4(b) shows marginally clearer evidence for a decreasing number of category 1 storms as forcing increases. The inset shows the simulations' results alone to illustrate this more clearly and Figures 4(c-d) shows for category 3 and 4 storms, there

https://doi.org/10.5194/egusphere-2023-1694
Preprint. Discussion started: 1 August 2023

Dataset	Description
ERA5	Reanalysis data (Hersbach et al., 2020)
UKESM1[_#2-16]	historical simulation data from the CMIP6 UKESM ensemble (Tang et al., 2019); r1i1p1f2, r2i1p1f2, r3i1p1f2, r4i1p1f2, r5i1p1f3, r6i1p1f3, r7i1p1f3, r8i1p1f2, r9i1p1f2, r10i1p1f2, r11i1p1f2, r12i1p1f2, r16i1p1f2, r17i1p1f2, r18i1p1f2, r19i1p1f2.
UKESM1_NZ	UKESM run by present authors using starting conditions from UKESM historical simulation `r4i1p1f2` at 01/01/1950 (Tang et al., 2019)
NZESM_WITHOUT_⋯ PHOTOLYSIS_CHANGE	NZESM, omitting solar-cycle dependence of photolysis (Dennison et al., 2019) starting from UKESM historical simulation `r4i1p1f2`, 01/01/1950 (Tang et al., 2019)
NZESM	1×NZESM using starting conditions from UKESM historical simulation `r4i1p1f2`, 01/01/1950 (Tang et al., 2019).
NZESM#2,3	2×NZESM started from 01/01/1940 (starting from `r17i1p1f2` and `r12i1p1f2` respectively)
NZESM#4	1×NZESM started from 01/01/1851 (`r17i1p1f2`)
NZESM_SSP126[_#2-3]	3×NZESM SSP1-2.6 scenario (Behrens et al., 2022).
NZESM_SSP245[_#2-3]	3×NZESM SSP2-4.5 scenario (Behrens et al., 2022).
NZESM_SSP370[_#2-3]	3×NZESM SSP3-7.0 scenario (Behrens et al., 2022).
UKESM1_SSP126[_#2-5]	5×UKESM SSP1-2.6 scenario (Good et al., 2019a); `r1i1p1f2, r2i1p1f2, r3i1p1f2, r4i1p1f2, r8i1p1f2.`
UKESM1_SSP245[_#2-5]	5×UKESM SSP2-4.5 scenario (Good et al., 2019b); `r1i1p1f2, r2i1p1f2, r3i1p1f2, r4i1p1f2, r8i1p1f2.`
UKESM1_SSP370[_#2-5]	5×UKESM SSP3-7.0 scenario (Good et al., 2019c); `r1i1p1f2. r2i1p1f2, r3i1p1f2, r4i1p1f2, r8i1p1f2.`
UKESM1_SSP585[_#2-5]	5×UKESM SSP5-8.5 scenario (Good et al., 2019d); `r1i1p1f2, r2i1p1f2, r3i1p1f2, r4i1p1f2, r8i1p1f2.`

Table 3. Datasets used in Figures 4. All SSP data is for 2080-2099 inclusive and all historical data is 1989-2008 inclusive. Simulation identifiers of the form $\underline{\mathrm{r}}\alpha\underline{\mathrm{i}}\beta\underline{\mathrm{p}}\gamma\underline{\mathrm{f}}\delta$ indicate the realisation, initialisation, physics and forcing for each ensemble member, e.g. (Zhao et al., 2022) or https://pcmdi.llnl.gov/CMIP6/Guide/modelers.html. 'Hashtag' (#) symbols indicate ensemble member number indices.

https://doi.org/10.5194/egusphere-2023-1694
Preprint. Discussion started: 1 August 2023

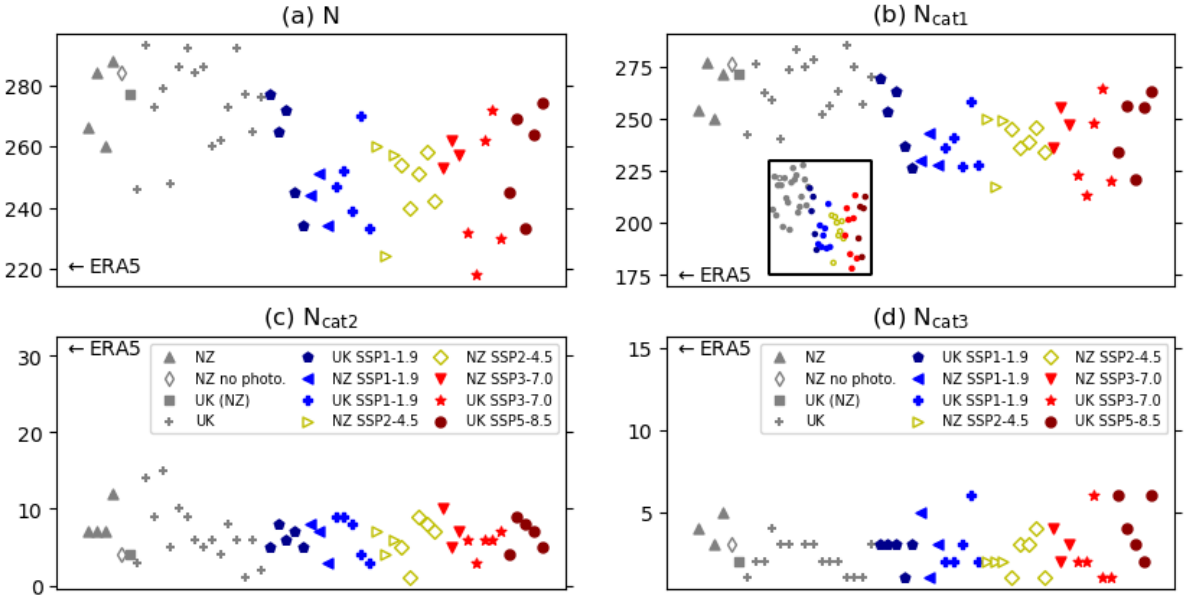

Figure 4. Total number N (a) and decomposition by storm category (b-d) for the situation shown in Figure 1. Only categories 1-3 are shown since the number in category 4 are almost universally 0 or 1; three cases have 2 and two have 3 and so basing any conclusions on such low numbers is dubious at best. The inset to (b) shows the simulations' alone, colour-coded the same way as the main figure and with all circle as markers to aid the eye.

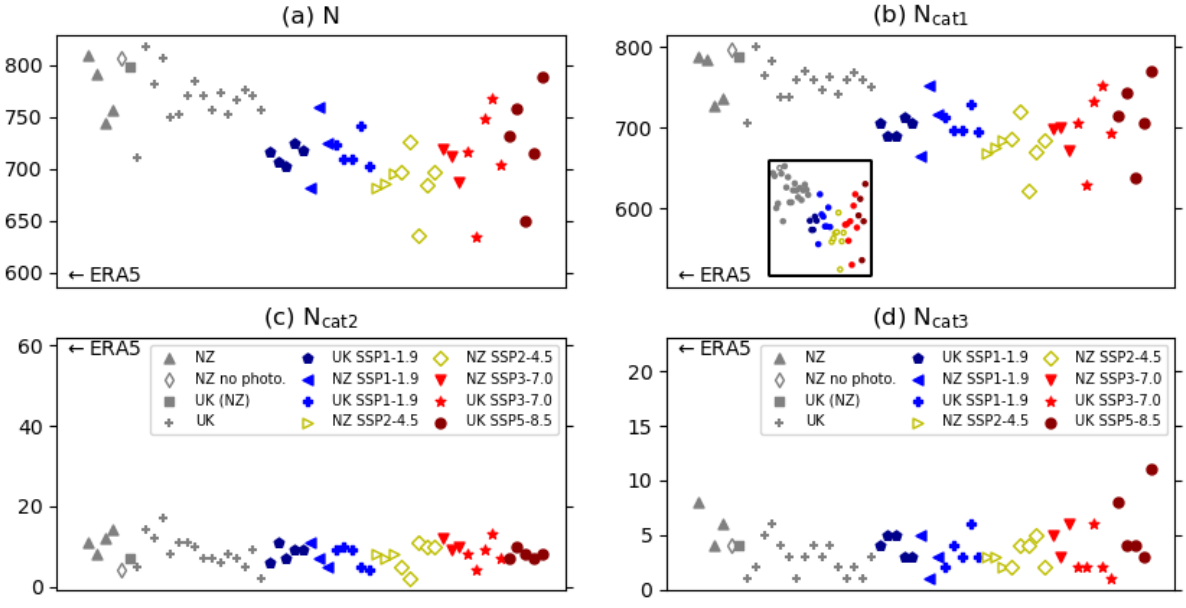

Figure 5. As for Figure 4 but globally. The numbers of category 4 storms is still too low to draw conclusions from.

https://doi.org/10.5194/egusphere-2023-1694
Preprint. Discussion started: 1 August 2023

are not enough systems detected for any putative conclusions to be drawn regarding frequency versus $\mathcal{F}$. The lack of any discernible difference between the numbers given by the NZESM and UKESM is an interesting result and is far from obvious. Indeed our initial expectation was that there would be a non-negligible difference in the overall cycle occurrence frequency in the two models given the substantially different surface ocean physics.

To try and draw more statistically robust conclusions, Figure 5 shows the same situation as for Figure 4 but for all longitudes. Comparing Figures 4(a) and 5(a) shows that approximately a third of the global tropical cycles have their genesis in the region considered in Figure 1. We also see that there is, again, a general decrease in N as forcing increases.

At extreme forcing levels though – SSP5-8.5; the dark red circles in Figure 5(a) – there is some indication that N may actually start to *increase* again, albeit to a level somewhat lower than in the historical period. This behaviour is also seen for N_{cat1} and N_{cat3} although the numbers of category 3 systems are very low, averaging only 1 per 4 years or so. There is no change in N_{cat2} for either the regional or the global case and the relative over/under estimation compared to ERA5 is the same in both cases.

In both the regional and global cases, the frequency of the more damaging systems is underestimated and represents a target for future cyclone tracking algorithms. Indeed, ERA5 itself tends to underestimate the strong tropical cyclones (Ullrich et al., 2021) and so care should be taken when interpreting the results presented here too precisely.

All of the historical simulations performed by the present authors fall well within the ranges of UKESM1 historical ensemble and so to remove any potential model dependency in the results that follow, only UKESM1 historical ensemble simulations are included going forward. We use 5-member ensembles for all SSP results below to enable us to compare similar numbers of simulations for each forcing scenario; the number of UKESM historical ensemble members is considerably larger than any of the SSPs.

We now move on to discuss the potential changes to TC strength with climate change.

5.2 Power dissipation index of tropical cyclones

In this section we illustrate one possibility to quantify the potential change to damage caused by tropical cyclones; that of the power dissipation index, PDI. We use the definition in (Emanuel, 2005),

$$\mathrm{PDI} \equiv \int_0^\tau \mathcal{V}_{max}^3 \mathrm{d}t, \tag{1}$$

where PDI is the power dissipation index and $\mathcal{V}_{max}$ is the maximum wind speed in the time resolution of the input data. Strictly speaking $\mathcal{V}_{max}$ is the maximum *sustained* windspeed within the physics timestep of the model; this is 20 minutes in UKESM1 and so this is the minimum time within which $\mathcal{V}_{max}$ can be said to be 'sustained'.

https://doi.org/10.5194/egusphere-2023-1694
Preprint. Discussion started: 1 August 2023

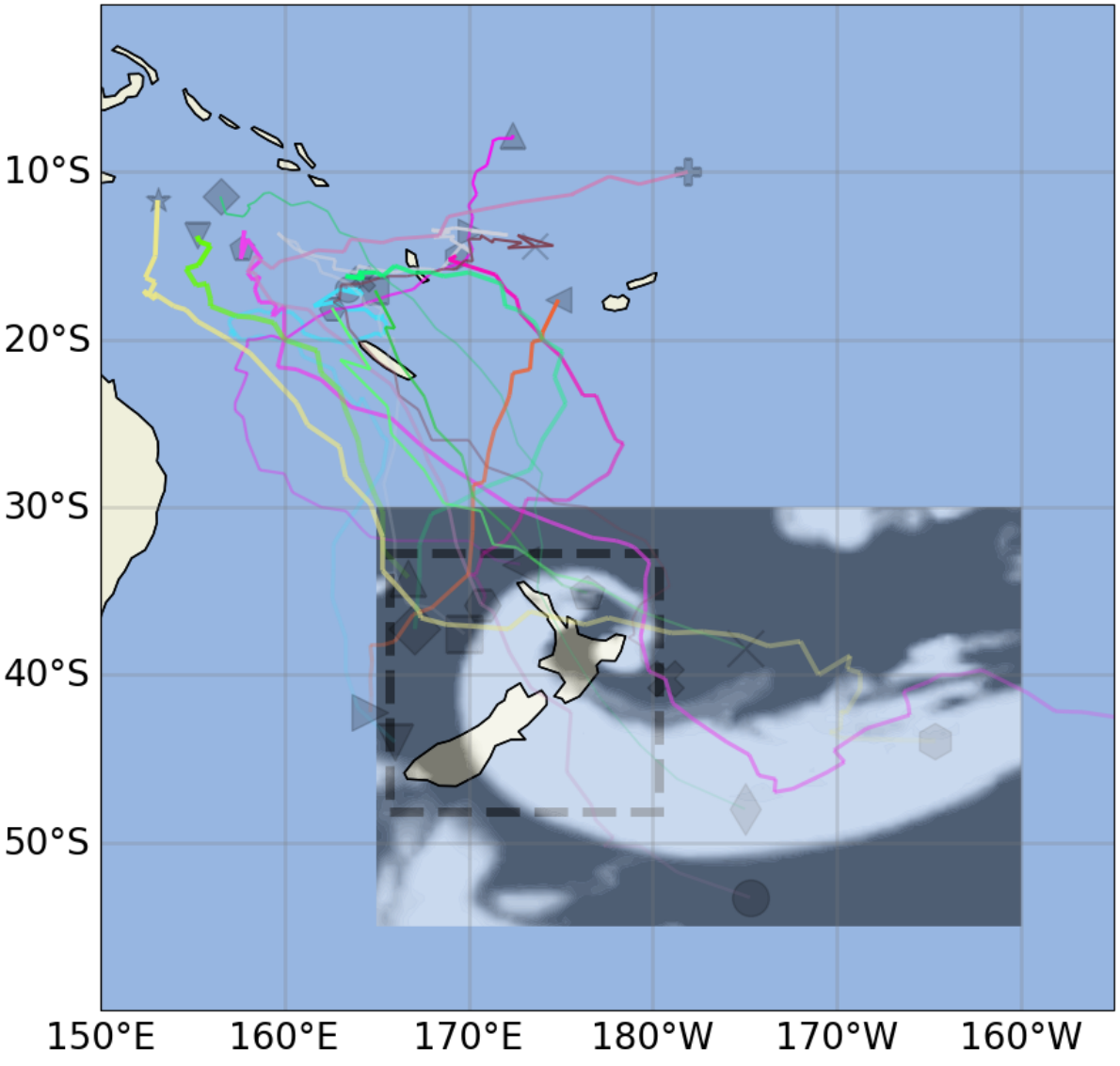

Figure 6. All ERA5 cyclones formed from -20° to 0° in 1989 – 2008 which 'hit' New Zealand at some point in their history as indicated by the dashed box. The colours are arbitrary and are merely present to differentiate between different systems. The transparency of the plotted lines also decreases from 1 at genesis to 0.1 at termination. The overlaying image over the New Zealand region is the medium height cloud cover from the ERA5 reanalysis at `20230214T0000Z` and shows the huge spatial extent of tropical cyclone Gabrielle which caused widespread destruction and loss of life. The characteristic clockwise rotation around the low pressure centre is clearly visible.

https://doi.org/10.5194/egusphere-2023-1694
Preprint. Discussion started: 1 August 2023

5.2.1 Tropical cyclones in the New Zealand sector

We have used latitude bands for genesis and intersection rather than specifically concentrating on systems that 'hit' New Zealand because this makes the numbers available to study too small. Figure 6 shows the all tropical cyclones generated between the equator and -20° during 1989-2008 which hit New Zealand and clearly there are not enough of them to be able to make any meaningful, statistical conclusions about the changes to this number as the climate changes.

Firstly we consider tropical cyclones which are generated in the tropical AGRIF region which intersect New Zealand latitudes (again in the AGRIF region). These systems are shown in Figure 7 and further illustrate why the statistics of storms impacting New Zealand specifically – dashed box in Figure 6 – are so sparse. For example in sub-Figures 7(p, r, x) there are no tropical cyclones which impact New Zealand.

Even though the statistics are sparse it is of interest to examine this specific case to try and understand what information can be gleaned from wind speeds along the entire track – every 6 hours – rather than simply counting cyclone occurrence, which clearly only yields one datum per system. We also consider all SSPs to quantify the projected change to cyclone damage potential in a warming world.

Figure 8(a) shows the mean, each of the ensemble members and intra-ensemble spread of the PDI for the 5-member ensembles at each SSP in Figure 7 as well as a comparable 5-member historical ensemble. The ensemble spread is large, as reflected by the broadly-overlapping error bars. There is however a clear relationship between PDI and $\mathcal{F}$. Indeed, this shows that an increase in PDI per storm of up to 24% in the New Zealand sector may be expected by 2100 assuming a 'worst case' scenario, SSP5-8.5. The large spread of the results, particularly for SSP1-1.9 illustrates why the mean PDI is non-monotonically increasing with $\mathcal{F}$; i.e. one ensemble member has a PDI which is significantly higher than the other 4. Larger regions are considered below and once enough TCs are counted to improve the statistics, the monotonic behaviour emerges, e.g. Figure 10(e-f).

In Figure 8(b), we recast the data in Figure 8(a) to take into account the unequal spacing in the $\mathcal{F}$ values for each SSP. We also perform a linear fit to the data so that we can obtain a rough quantification of the increase in potential future storm damage and in this case the linearity of fit parameter, R^2=0.78.

The gradient of the linear fit in Figure 8(b) is represented by equation 2

$$\frac{\mathrm{d\,PDI}}{\mathrm{d}\mathcal{F}} \approx 1.5 \times 10^7 \left[\mathrm{m}^3 \cdot \mathrm{kg}^{-1} \cdot \mathrm{s}\right] \tag{2}$$

Equation 2 says that for every 1 $\mathrm{W} \cdot \mathrm{m}^{-2}$ increase in the top of atmosphere radiative forcing, $\mathcal{F}$ there is an associated increase in the PDI, of $1.5 \times 10^7 \left[\mathrm{m}^3 \cdot \mathrm{kg}^{-1} \cdot \mathrm{s}\right]$ per tropical cyclone impacting New Zealand latitudes.

We now perform the same analysis at all longitudes to attempt to improve the statistics of the analysis.

5.2.2 Global tropical cyclones

Figure 9 shows the tropical cyclone tracks for the entire southern hemisphere and for the same models as Figure 7 and using the same latitude criteria. In general the distribution of tropical cyclones in the models is in good agreement with the ERA5

https://doi.org/10.5194/egusphere-2023-1694
Preprint. Discussion started: 1 August 2023

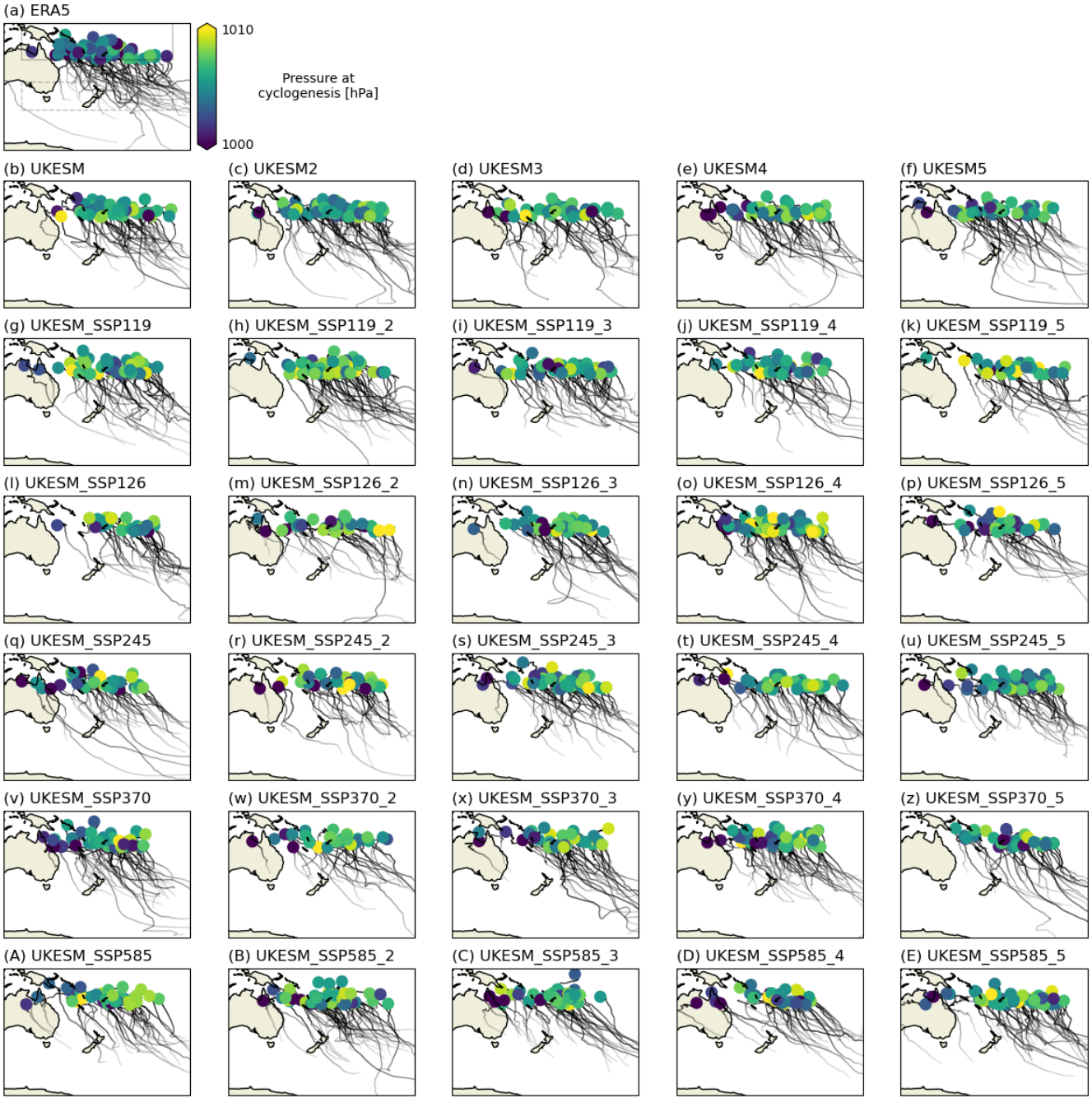

Figure 7. Cyclones formed in the solid box region in (a) which intersect the dashed box region. Both boxes have the same longitude extent as the AGRIF region, the solid line box goes from the equator to -20° S and the dashed line box goes from -48.17° to -32.75° S. The pressure at cyclogenesis is shown and the colour bar is the same for all simulations and the transparency of the plotted cyclone tracks decreases from 1 at genesis to 0.1 at termination.The datasets are ERA5 and the following UKESM simulations (a), historical (b)-(f), SSP1-1.9 (g)-(k), SSP1-2.6 (l)-(p), SSP2-4.5 (q)-(u), SSP3-7.0 (v)-(z) and SSP5-8.5 (A)-(E).

https://doi.org/10.5194/egusphere-2023-1694
Preprint. Discussion started: 1 August 2023

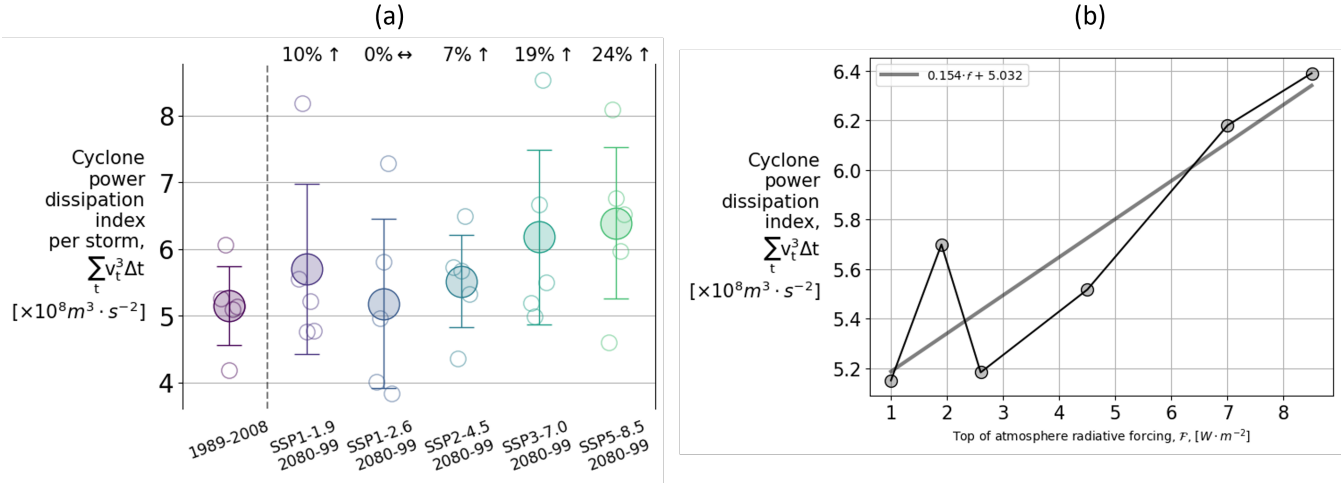

Figure 8. (a) Cyclone power dissipation index – PDI – *per storm* for the simulated systems shown in Figure 7. (a) Shows the ensemble mean, the 5 individual ensemble members, and ± 1 standard. (b) Mean PDI as a function of the top of atmosphere radiative forcing, $\mathcal{F}$. The best fit line has an R^2 value of 0.78.

reanalysis – Figure 9(a) – reproducing several salient features, for example the almost complete absence of South Atlantic tropical cyclones. The paucity of storms in this basin is thought to be due to, for example, excessive wind shear in the vertical (Pezza and Simmonds, 2005) and low sea surface temperatures (Evans and Braun, 2012).

As for the destructive power of these Southern Hemisphere storms, Figure 10(a) shows the PDI per storm, PDI, for each SSP and Figure 10(d) as a function of $\mathcal{F}$.

As was the goal with using a larger longitude range, the error bars in Figure 10(a) are – in general – smaller than in Figure 8(a). In addition to the reduction in the error bar size, we see that when a larger population of storms is considered, R^2 also increases; from 0.78 in Figure 10(d) to 0.92 in Figure 8(b).

It is increased still further to 0.95 when the southern boundary of the tropical genesis region under consideration is widened to -25° – Figure 10(e) – and is accompanied by a shift to exclusively monotonic increases in mean PDI with $\mathcal{F}$ – Figure 10(b). This increase in linearity-of-fit however is accompanied by a reduction in the gradient of increase in PDI and is indeed reduced even further when the southward boundary of the genesis region is set to -30°. It is thought that this reduction in upward gradient is due to the steady inclusion of extra-tropical systems – in terms of their genesis mechanisms – which are presumed to be essentially absent equatorward of -20°.

5.2.3 Effect of cyclogenesis region on frequency of storms delineated by category

Finally in this section, we separate the storms shown in Figures 7 and 9 into their Saffir-Simpson categories. The data are shown in Figure 11 and Table A1 in Appendix B, which also shows more explicitly where projected future numbers of TCs are projected to increase or decrease with respect to historical numbers.

https://doi.org/10.5194/egusphere-2023-1694
Preprint. Discussion started: 1 August 2023

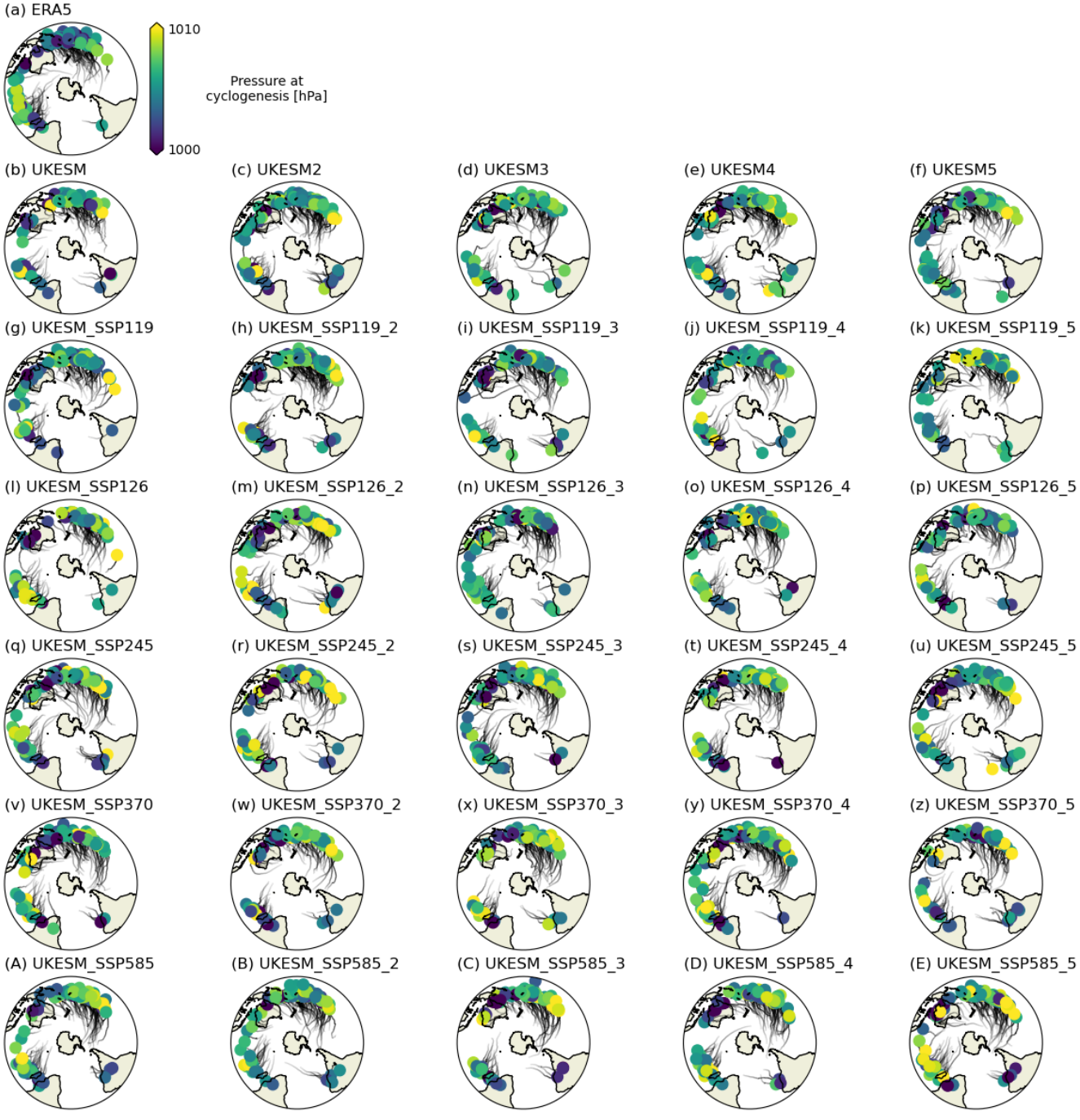

Figure 9. As for Figure 7 but globally. The datasets are ERA5 and the following UKESM simulations (a), historical (b)-(f), SSP1-1.9 (g)-(k), SSP1-2.6 (l)-(p), SSP2-4.5 (q)-(u), SSP3-7.0 (v)-(z) and SSP5-8.5 (A)-(E). The colour bar is the same for all simulations and the transparency of the plotted lines decreases from 1 at genesis to 0.1 at termination.

https://doi.org/10.5194/egusphere-2023-1694
Preprint. Discussion started: 1 August 2023

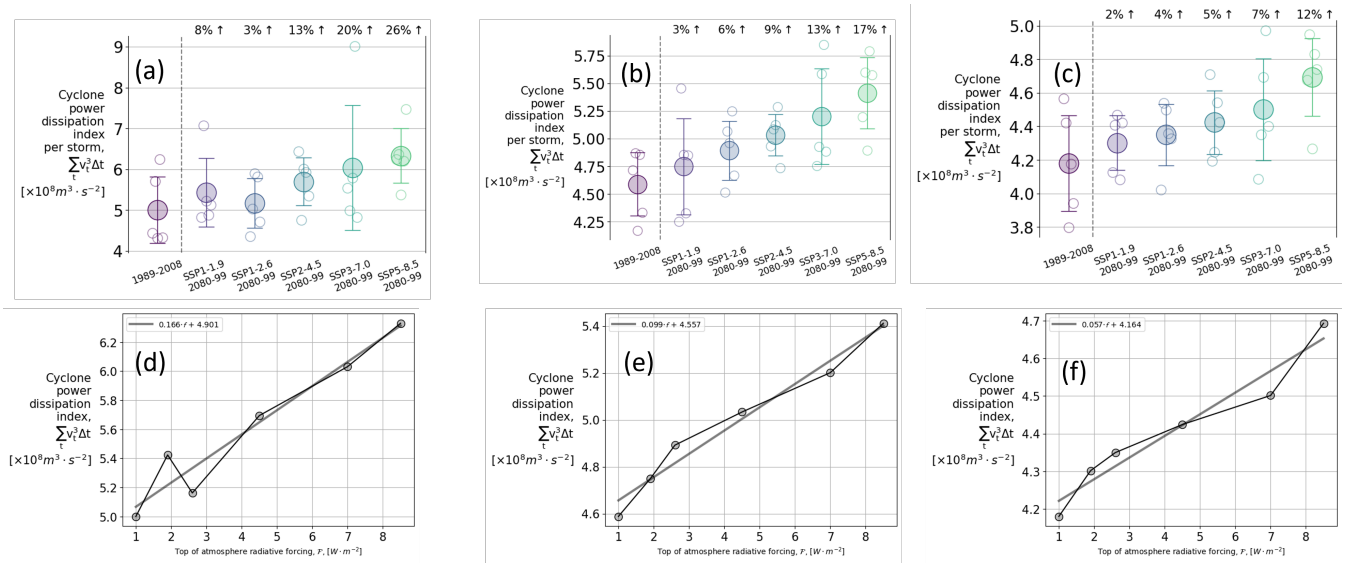

Figure 10. Mean $\pm$ 1 standard deviation - σ - cyclone power dissipation index – PDI – *per storm* for the simulated systems shown in Figure 9 (a) and extending the southern boundary of the genesis region to -25° (b) and -30° (c) respectively. (d) - (f) show the mean PDI as in (a) - (c) but against $\mathcal{F}$ on the x-axis; a linear fit is also shown and the R^2 goodness of fit parameter is 0.92, 0.95 and 0.90 for (d-f) respectively.

One aspect of this data which is particularly striking is the convergence in the ability of the simulations – and tracking software – to more accurately reproduce the number of cyclones in ERA5 as the size of the cyclogenesis region is increased. Consider Figure 11(a,b) compared to 11(c,d) for example where N_{cat2} and N_{cat3} are well-simulated in the latter pair but are noticeably overestimated in the former. This is clearly a statistical effect because as the size of the genesis region considered increases, the more likely the model is to detect these relatively rare events.

Figure 11 also quantifies of the size of the region necessary to resolved the 'long tail' of high-impact, low-probability events reaching mid-latitudes. Indeed no category 4 systems are tracked within 20° of the equator in this analysis.

We also see that the general underestimation in N in Figure 11(a) is alleviated when using larger regions. This underestimation is the reverse to that seen above when no termination criterion was imposed, i.e. Figures 4 & 5. This tells us that, in general, the tracking software is 'losing' too many cyclones too quickly after detection and is an area of possible improvement to be targeted in future work.

In the next section we examine the physical reasons for the projected increase in tropical cyclone power dissipation discussed above.

5.3 What factors influence tropical cyclone frequency and severity?

As discussed above, estimating the number of tropical cyclones in the Southern Hemisphere with climate change is challenging, however it is a robust result that they are predicted to be stronger, (Walsh et al., 2016; Knutson et al., 2010; Emanuel, 2005).

https://doi.org/10.5194/egusphere-2023-1694
Preprint. Discussion started: 1 August 2023

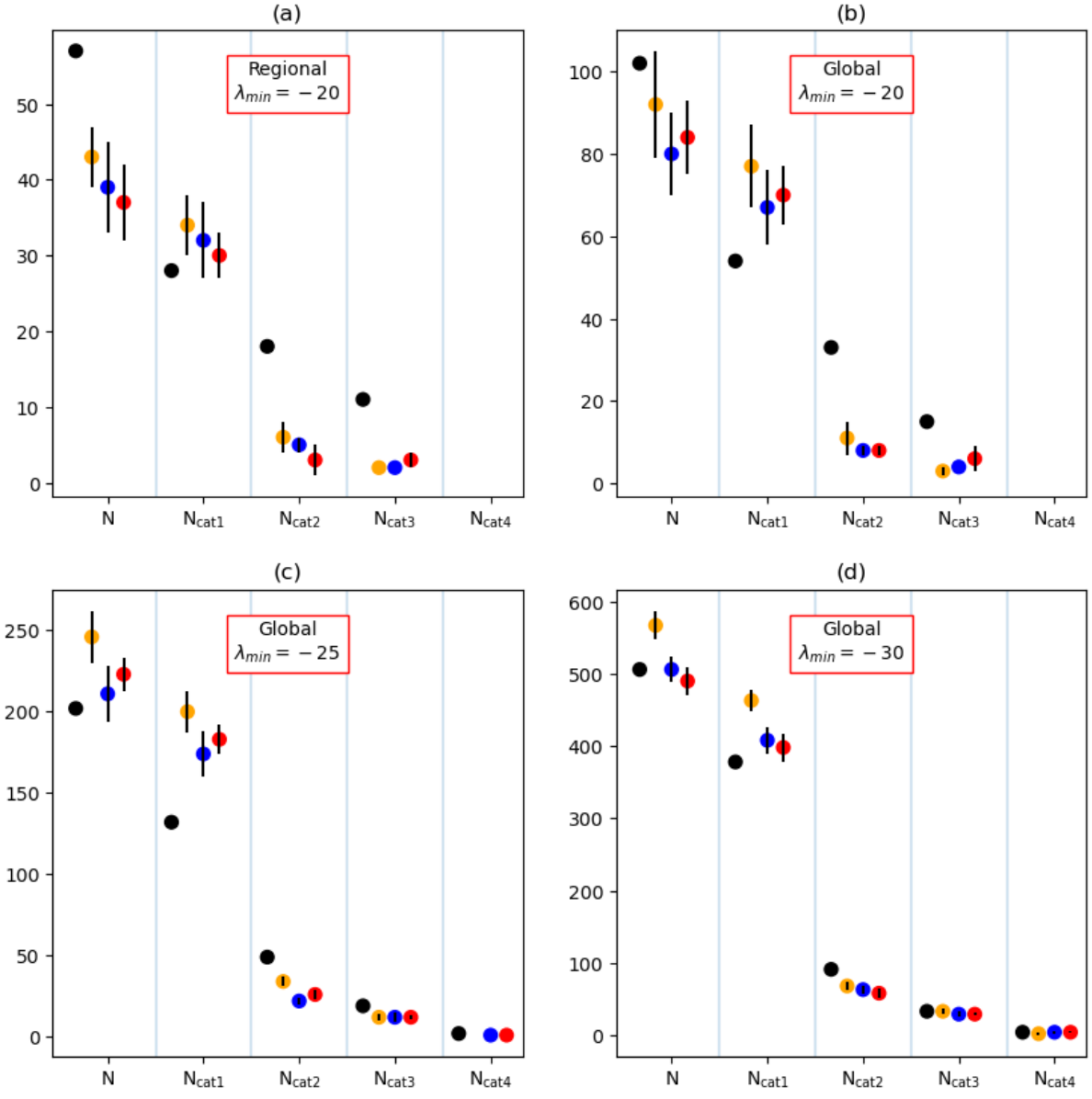

Figure 11. Cyclone counts from the area criteria in: (a) Figure 7, (b) Figure 9, (c,d) Figure 9 but with the southern boundary of the genesis region extended to -25° and -30° respectively. With each category (total, N, category 1, etc) the black marker shows the ERA5 results, orange is historical, blue is SSP1-1.9 and red is SSP5-8.5. The vertical bars show ± one standard deviation within the 5 member ensembles considered.

https://doi.org/10.5194/egusphere-2023-1694
Preprint. Discussion started: 1 August 2023

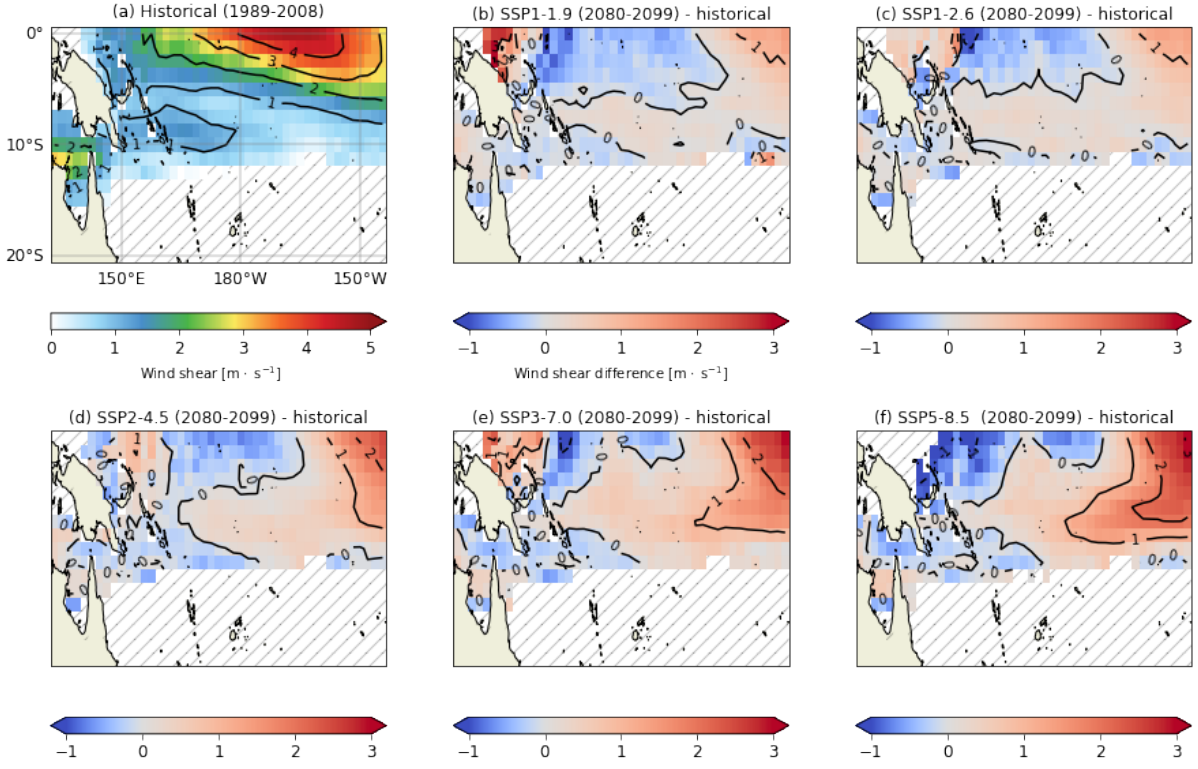

Figure 12. Wind shear over ocean (a) and projected wind shear change with respect to (a) for 0° to -20° S and 132.7° E to 216.3° E for (a) historical (1989-2008), (b) SSP1-1.9, (c) SSP1-2.6, (d) SSP2-4.5, (e) SSP3-7.0 and (f) SSP5-8.5. All data are means of the 5 member ensembles considered above and all negative values are masked.

There are several – related – conditions for tropical cyclogenesis, e.g. high SST (Dare and McBride, 2011) and humidity (Wu et al., 2012) (also see (Lang, 2023) for a discussion on the problems that GCMs have in modelling tropical relative humidity in the first place) and sufficiently small vertical wind shear (Vecchi and Soden, 2007). In this section we examine each of these as predictors of tropical cyclone frequency.

5.3.1 Wind shear

We use the definition for vertical wind shear in (Vecchi and Soden, 2007), which is the difference in wind speed magnitude between 850 and 200hPa.

Figure 12(a) shows the historical UKESM wind shear and 12(b-f) show the project changes for the five SSPs with respect to the historical period for the AGRIF region.

There is a clear increase in the wind shear across the AGRIF region shown in Figure 12 although this is not spatially uniform, with the clearest increase in wind shear occurring in the northeast of the region considered. This trend becomes clearer when the area mean is considered, Figure 13(a). Figure 13(b) shows the same analysis but for all longitudes. The result is the same,

https://doi.org/10.5194/egusphere-2023-1694
Preprint. Discussion started: 1 August 2023

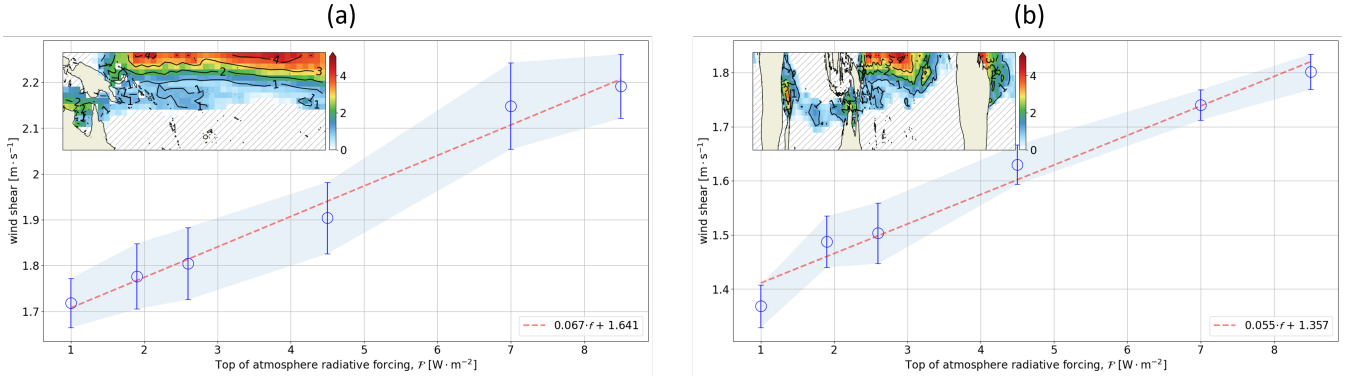

Figure 13. (a) Area mean wind shear for 0° to -20° S and 132.7° E to 216.3° E. Negative values are masked and the error bars and shading show ± 1 standard deviation of the 5 member ensemble means for each scenario. Inset; Annual wind shear map for 1989-2008 for the first historical ensemble member used. (b) As for (a) but for all longitudes. Note the different y-axis scale.

i.e. that wind shear increases as radiative forcing increases and therefore – at least partly – explains the reason for the reduction in tropical cyclone numbers seen above.

5.3.2 Relative humidity

Figure 14 shows the ensemble, zonal mean relative humidity – RH – as a function of pressure between -30° and the equator for; (a) the historical simulations, 1989-2008 and; (b-f) SSPs 1-5 with respect to (a). We have masked values above the tropopause since it is tropospheric humidity which dictates cyclogenesis.

In contrast to the wind shear in Figures 12 and 13 the relationship between tropospheric RH and $\mathcal{F}$ is far from linear and of course is three-dimensional rather than two. There are certain tendencies in the RH distribution which are clear however, such as the decreases around 800 and 250hPa and the low-latitude increase around 500hPa. These persistent features notwithstanding, it is clearly very difficult to assign any potential change in tropical cyclone genesis frequency to that of RH in these results, which aligns with the general uncertainty around changes to TC frequencies in the future.

5.3.3 Surface heat fluxes

Although it is far from obvious that the combined effects of changing wind shear and RH will tend to increase or decrease tropical cyclogenesis frequency under all circumstances, it is much clearer that whatever cyclones do occur will be stronger as $\mathcal{F}$ increases. In this section we give a quantification of the surface upward heat transfer available between the equator and the south of New Zealand. Figure 15(a) shows the area-integrated heat transfer across all longitudes for the region shown in the inset and sub-Figures (b)-(g) show SSTs.

Figure 15(a) shows the average surface upward heat transfer between -48° and the equator. The increase is of course expected – although the linearity is particularly striking – but it gives an illustration of one measure of the 'fuel' available for tropical

https://doi.org/10.5194/egusphere-2023-1694
Preprint. Discussion started: 1 August 2023

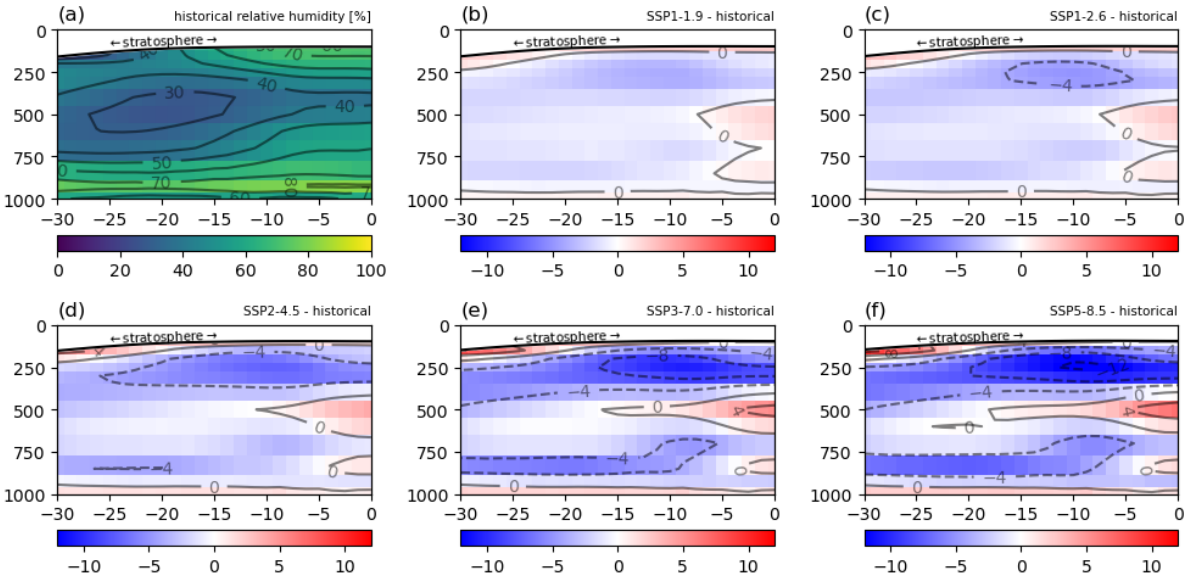

Figure 14. The ensemble, zonal mean relative humidity [%] for; (a) the historical simulations, 1989-2008 and; (b-f) SSPs 1-5 with respect to (a). Values above the tropopause are masked. The latitude range in -30° to 0°.

cyclones and hence explains why tropical cyclones are expected to strengthen in the future even though their number may decrease.

To give a more nuanced view Figures 15(b-g) show the SSTs and the 26.5° C isotherm, which is often used as a threshold temperature for tropical cyclogenesis (see (McTaggart-Cowan et al., 2015) for an in-depth discussion on this). As well as the inexorable rise in overall SST with greenhouse gas forcing, the region bounded from below by the 26.5° C covers almost the entire area considered by the time SSP5-8.5 is shown in Figure 15(g). On its own, the expansion of the region with SST greater than 26.5° C would tend to increase the number of TCs formed. However we have seen consistently that tropical cyclone numbers are relatively insensitive to forcing and indeed if anything show a decrease in their number as global warming increases, with the exception of extreme forcing, see e.g. Figure 5(a). It is possible therefore that the simulations' tendency to shown an increase in the number of TCs at extreme warming scenarios is due to this increase in the region of ocean exhibiting SSTs greater than 26.5° C.

With the information that we have now gleaned from studying RH, wind shear, the position of the threshold SST for tropical cyclogenesis and the surface upward radiation balance, the projected increase in TC strength with climate change appears robust. The projected *number* of TCs however, and in particular those affecting New Zealand is highly uncertain and governed by several related yet competing physical tendencies.

Although not considered in this work, ocean heat content and its effect on future marine heatwaves is a field of intense contemporary study (Behrens et al., 2022; Walsh et al., 2018; Frölicher and Laufkötter, 2018). It would be of significant interest to study these two inter-related phenomena in a combined fashion, particularly if they were to coincide in a future

https://doi.org/10.5194/egusphere-2023-1694
Preprint. Discussion started: 1 August 2023

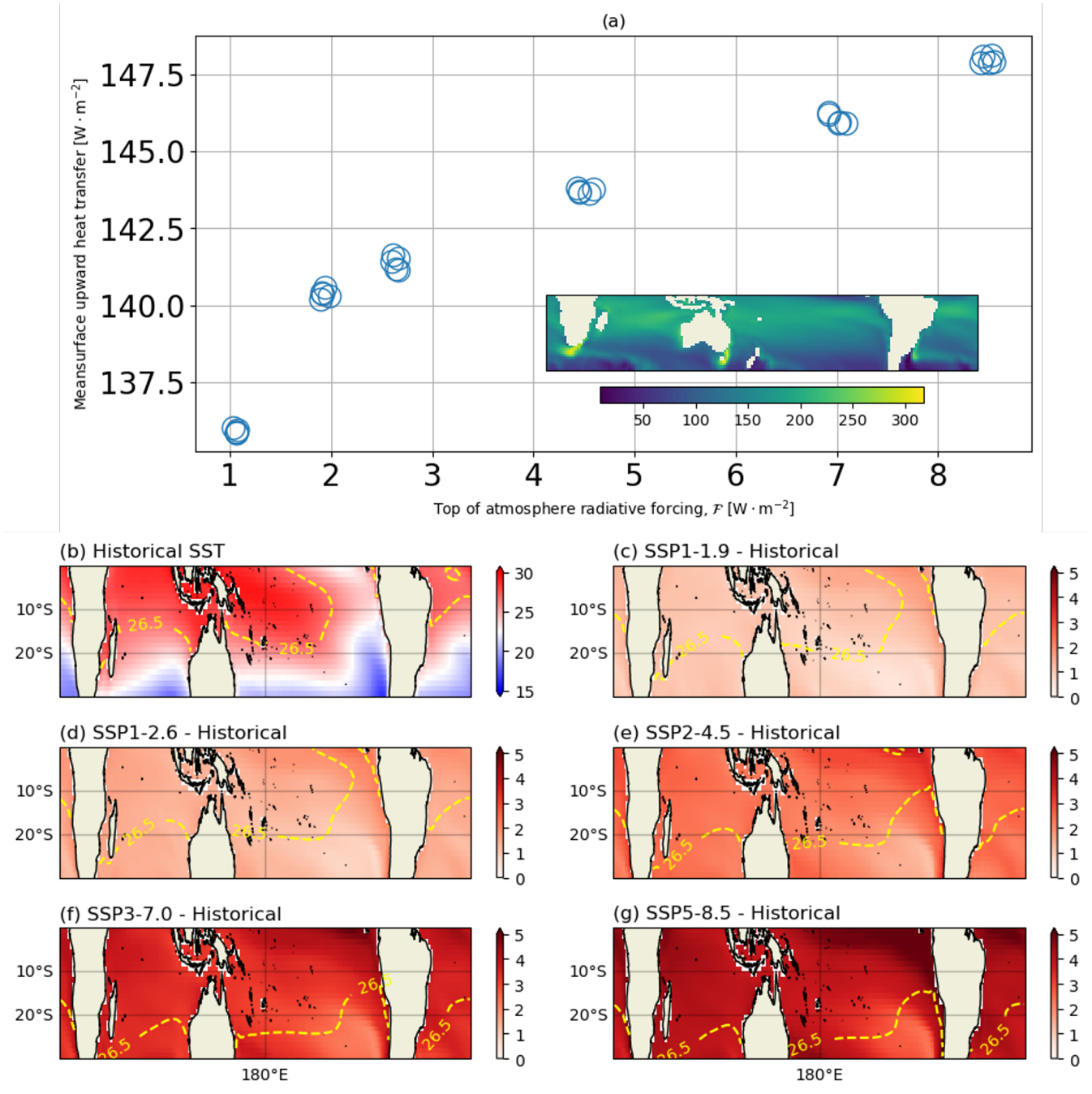

Figure 15. (a) Area integrated surface upward heat transfer for the area in the inset figure (-48° to the equator). A small amount of noise has been introduced into the $\mathcal{F}$ values to make it easier to see the individual symbols. The $\mathcal{F}$ values are 1 (approximate value for 1989-2008), 1.9, 2.6, 4.5, 6.0 and 8.5 W · m^{-2}; (b) historical SSTs; (c-g) SSTs (reds) for SSPs 1-5 relative to the historical period. The 26.5° isotherms are shown for the historical period and each of the SSPs as per the sub-figure titles.

https://doi.org/10.5194/egusphere-2023-1694
Preprint. Discussion started: 1 August 2023

involving 'compound extremes' where multiple different variables (humidity and temperature, e.g. (Fischer and Knutti, 2013); rainfall, temperature and high tides e.g. (Benestad and Haugen, 2007)) reinforce one another.

6 Conclusions

In this manuscript we have examined the storm climatologies of two related climate models, and two reanalysis products using the open source `stormTracking` package. This package was validated by comparison with another package – `tempestExtremes` – and by its ability to reproduce the observed track of cyclones Giselle (April 1968) and Gabrielle (February 2023).

We use two, related, state-of-the-art coupled climate models in this study; The United Kingdom Earth System Model, Version 1 – UKESM1 – and the New Zealand Earth System Model, NZESM. The latter is a sibling model of the former and the main difference between the two is the presence of a regional, two-way-nested, eddy-permitting ocean model in the New Zealand region.

The climate models considered were UKESM1 and the NZESM, and due to the agreement of the results obtained from the two models (plus the lack of sensitivity to ozone photolysis, hardware and compiler types, and spinup time) only UKESM1 was considered in future projections due to the availability of larger ensemble sizes for each SSP and the wider range of forcing scenarios. It would be of interest in future work to explicitly consider the different between the NZESM and UKESM1 in future projections in future work.

When all TCs produced from the entire model ensemble were considered the models overestimate N and N_{cat1}. The reverse is seen for higher category storms however. In general, there is a tendency for the number of TCs to decrease except at very high forcing scenarios where there is some tentative evidence of an increase. This is possibly due to the fraction of ocean having a surface temperature above the generally-accepted threshold of 26.5° being so large that other factors tending to reduce TC numbers – e.g. wind shear – are overwhelmed.

For tropical cyclones with their genesis in the AGRIF region which hit New Zealand latitudes there is a clear increase, albeit with significant uncertainty, in the and mean PDI per storm as the amount of forcing is increased. In this particular example, we project changes of up to approximately 25% by 2100. To reduce the size of the spread for these measures of PDI, we then considered all longitudes and found that the ensemble spread was reduced in the mean; that is, the error bars in Figure 10(a) are smaller than those in Figure 8(a).

As the width of the TC genesis band was increased, the linearity of the projected increase in PDI with climate forcing increases from 0.78 for the New Zealand region alone to 0.92 when all latitudes are considered. This is increased still further to 0.95 for genesis latitudes equatorward of -25°S and reduces slightly to 0.90 for the -30° case. As the lower boundary of the genesis region moves southward there is a noticeable reduction in the PDI gradient with forcing and a reduction in the magnitude of the mean PDI itself. This is because the most damaging systems tend to originate close to the equator and so considering systems outside of the 'high-tropics' will tend to include more and more systems whose genesis is not purely governed by the physical processes which define tropical systems in the first place.

https://doi.org/10.5194/egusphere-2023-1694
Preprint. Discussion started: 1 August 2023

When examining these TCs which cross New Zealand latitudes by Saffir-Simpson category, there is a general underestimation in N when only the New Zealand region is considered. This is not the case for larger regions when the statistics become more robust. This underestimation is the reverse of that seen when considering all TCs, irrespective of their destination and shows that the tracking software has a tendency to 'lose' too many TCs too quickly in their evolution. This analysis also shows evidence for underestimation of category 2 and 3 TCs unless latitude bands wider than 20° are considered plus an inability to track any category 4 systems under the same conditions.

Tropical cyclogenesis involves a highly-complex and coupled set of conditions to be fulfilled and our results show that the decrease in tropical cyclone occurrence is related to the increase in tropical wind shear in a quasi-linear fashion. When the tropospheric humidity is considered however, drawing conclusions is made more difficult by changes of different signs to the humidity at different levels. Furthermore, when considering the area of the tropical oceans which have SSTs of at least 26.5°C, we might expect the number of tropical cyclones to increase with forcing; the reverse of what is seen in our simulations except at extreme levels of TOA forcing where almost the entire tropics have SST greater than the required threshold.

The increase in the damage potential of future tropical cyclones appears primarily due to the increase in the availability of heat flux from the ocean surface. This is of course expected from thermodynamic arguments, however this study does not address potential future changes to cyclone impacts from compound extremes. This complexity arises in events where multiple types of hazards arise, e.g. hide tides and high winds occurring either simultaneously or from the serial grouping of consecutive cyclones. In this latter case, authorities' and communities' ability to respond to new circumstances is made more challenging by the resources already pooled into dealing with the former. These combined and grouped hazards are potentially highly non-linear in their impacts and a future dedicated study thereof would be both societal and financial benefit.

Code and data availability. The `stormTracking` and `tempestExtremes` codes are available on GitHub at https://github.com/ecjoliver/stormTracking and https://github.com/ClimateGlobalChange/tempestextremes respectively. All UKESM1 data is available through the CMIP6 data archive at the Earth System grid Federation, https://esgf.llnl.gov/. The code describing the implementation of the AGRIF high-resolution ocean is available at Zenodo (Behrens, 2020)

Appendix A: Data from Figure 11

Table A1 shows the numerical data plotted in Figure 11.

Appendix B: Generation of storm climatologies

The method used in this study to firstly detect, and subsequently follow the trajectory of individual cyclones is described in detail in Chelton et al. (2011). Firstly, a regularly (horizontally) spaced, time series of sea-level pressure values is obtained and is regridded to 2° resolution, which is the default grid spacing in the software. Next, a detection algorithm is run on the data, which consists of:

https://doi.org/10.5194/egusphere-2023-1694
Preprint. Discussion started: 1 August 2023

Storm criteria	Forcing	N	N_{cat1}	N_{cat2}	N_{cat3}	N_{cat4}
	ERA5	57	28	18	11	–
Figure 7	hist.	43 ± 4	34 ± 4	6 ± 2	2	–
	SSP1-1.9	39 ± 6	32 ± 5	5 ± 1	2	–
	SSP5-8.5	37 ± 5	30 ± 3	3 ± 2	3 ± 1	–
	ERA5	102	54	33	15	–
Figure 9	hist.	92 ± 13	77 ± 10	11 ± 4	3 ± 1	–
	SSP1-1.9	80 ± 10	67 ± 9	8 ± 1	4	–
	SSP5-8.5	84 ± 9	70 ± 7	8 ± 1	6 ± 3	–
	ERA5	202	132	49	19	2
As for Figure 9 but to -25°S	hist.	246 ± 16	200 ± 13	34 ± 3	12 ± 2	–
	SSP1-1.9	211 ± 17	174 ± 14	$\Downarrow$ 22 ± 2	12 ± 3	$\Uparrow$ 1
	SSP5-8.5	223 ± 10	183 ± 9	26 ± 3	12 ± 1	1
	ERA5	506	378	91	33	4
As for Figure 9 but to -30°S	hist.	567 ± 20	463 ± 14	68 ± 6	33 ± 4	2 ± 2
	SSP1-1.9	$\Downarrow$ 506 ± 18	$\Downarrow$ 408 ± 18	63 ± 5	29 ± 4	4 ± 2
	SSP5-8.5	490 ± 20	398 ± 19	58 ± 6	29 ± 2	4 ± 1

Table A1. Cyclones counts and – where appropriate – ± 1 standard deviation for the conditions illustrated in Figures 7 and 9. Storm categories using the Saffir-Simpson scale pressure bounds, e.g. Song et al. (2010). The pressure bounds for categories 1-5 are: (1) $\forall\ P > 980$, (2) $965 < P_{min} < 980$, (3) $945 < P_{min} < 965$, (4) $920 < P_{min} < 945$ and (5) $P_{min} < 920$ respectively. Uncertainty estimates are not given where the mean standard deviation is less than 0.5 and hence rounded to zero. No category 5 storms were found in this work and N is not exactly equal to the sum of the individual categories due to integer rounding. The curly brackets indicate whether or not differents results' error bars overlap and the vertical arrows show the relative magnitude compared to those values not bracketed. This data is plotted in Figure 11.

1. Discretise the continuous pressure field into 200 equally-spaced value bins.
2. Finding closed regions of contours of SLP values.
3. Counting the number of data points ('pixels' in Chelton et al. (2011)) in the found region and rejecting it if it is too small. The threshold value used here is 9, again, the default value. Using the built-in value of 2°, a 3×3 square region corresponds to roughly 650×650 km^2.
4. Identify the region as anticyclonic if the region contains a maximum and cyclonic if it contains a minimum.
5. Find the average pressure ('amplitude' in Chelton et al. (2011)) of the bound region but don't count it if it is less than the value of the bin spacing – see item 1 – away from the mean in the region of interest.

https://doi.org/10.5194/egusphere-2023-1694
Preprint. Discussion started: 1 August 2023

This algorithm results in a list of storm latitude, longitude and amplitude which are then fed into a storm tracking algorithm.

1. Find storm centres within a region defined by a given maximum speed of propagation (i.e. 80km $\cdot$ hour^{-1}).
2. For the systems found in 1, choose the one closest to the coordinates in question.
3. Add the relevant metadata to the trajectory of the storm (coordinates, amplitude, time, date).
4. Delete the just-detected system from the list of 'possibles' for assignment in the next iteration of the algorithm.
5. Delete storms which (following Klotzbach et al. (2016)):
   (a) Are shorter than a threshold duration; which is equal to the timestep in the data in this work (default same as timestep in input data) .
   (b) Are shorter than a threshold total track length (default 1000km).
   (c) Have a distance from start to end which is 0.6 $\times$ the total track distance.

The only modifications made here are to convert the code from Python 2 to Python 3 coding standards. This change is purely structural and does not change any of the results obtained from the code.

Author contributions. JW, led the writing of the manuscript although all authors contributed. JW prepared the figures. JW and EB developed the high-resolution ocean model nesting and ran the NZESM and 'UKESM1_NZ' simulations. JT assisted with technical aspects of the porting of UKESM1 to the NIWA high-performance computer and interfaced with the wider Unified Model Partnership. OM oversees the ongoing NZESM project as a whole. PG provided the `tempestExtremes` data.

Competing interests. The authors declare no competing interests.

Acknowledgements. This paper obtained funding and support through the Ministry of Business Innovation and Employment Deep South National Science Challenge projects (C01X1412) and Royal Society Marsden Fund (NIW1701). The development of UKESM1, was supported by the Met Office Hadley Centre Climate Programme funded by BEIS and Defra (GA01101) and by the Natural Environment Research Council (NERC) national capability grant for the UK Earth System Modelling project, grant number NE/N017951/1. The authors would also like to acknowledge the support and collaboration of the wider Unified Model Partnership, https://www.metoffice.gov.uk/research/approach/collaboration/unified-model/partnership. and the use of New Zealand eScience Infrastructure (NeSI) high performance computing facilities, consulting support and training services as part of this research. New Zealand's national facilities are provided by NeSI and funded jointly by NeSI's collaborator institutions and through the Ministry of Business, Innovation & Employment's Research Infrastructure programme, www.nesi.org.nz.

https://doi.org/10.5194/egusphere-2023-1694
Preprint. Discussion started: 1 August 2023

References

Behrens, E.: erikbehrens/NZESM1: First release of the NZESM (ocean+sea ice code), https://doi.org/10.5281/zenodo.3873691, 2020.

Behrens, E., Williams, J., Morgenstern, O., Sutton, P., Rickard, G., and Williams, M. J.: Local grid refinement in New Zealand's earth system model: Tasman Sea ocean circulation improvements and super-gyre circulation implications, Journal of Advances in Modeling Earth Systems, 12, e2019MS001 996, 2020.

Behrens, E., Rickard, G., Rosier, S., Williams, J., Morgenstern, O., and Stone, D.: Projections of Future Marine Heatwaves for the Oceans Around New Zealand Using New Zealand's Earth System Model, Frontiers in Climate, p. 19, 2022.

Bell, B., Hersbach, H., Simmons, A., Berrisford, P., Dahlgren, P., Horányi, A., Muñoz-Sabater, J., Nicolas, J., Radu, R., Schepers, D., et al.: The ERA5 global reanalysis: Preliminary extension to 1950, Quarterly Journal of the Royal Meteorological Society, 147, 4186–4227, 2021.

Benestad, R. E. and Haugen, J. E.: On complex extremes: flood hazards and combined high spring-time precipitation and temperature in Norway, Climatic Change, 85, 381–406, 2007.

Cavicchia, L., Scoccimarro, E., Ascenso, G., Castelletti, A., Giuliani, M., and Gualdi, S.: Tropical Cyclone Genesis Potential Indices in a New High-Resolution Climate Models Ensemble: Limitations and Way Forward, Geophysical Research Letters, 50, e2023GL103 001, 2023.

Chand, S. S., Walsh, K. J., Camargo, S. J., Kossin, J. P., Tory, K. J., Wehner, M. F., Chan, J. C., Klotzbach, P. J., Dowdy, A. J., Bell, S. S., et al.: Declining tropical cyclone frequency under global warming, Nature Climate Change, 12, 655–661, 2022.

Chelton, D. B., Schlax, M. G., and Samelson, R. M.: Global observations of nonlinear mesoscale eddies, Progress in oceanography, 91, 167–216, 2011.

Compo, G. P., Whitaker, J. S., Sardeshmukh, P. D., Matsui, N., Allan, R. J., Yin, X., Gleason, B. E., Vose, R. S., Rutledge, G., Bessemoulin, P., Brönnimann, S., Brunet, M., Crouthamel, R. I., Grant, A. N., Groisman, P. Y., Jones, P. D., Kruk, M. C., Kruger, A. C., Marshall, G. J., Maugeri, M., Mok, H. Y., Nordli, , Ross, T. F., Trigo, R. M., Wang, X. L., Woodruff, S. D., and Worley, S. J.: The Twentieth Century Reanalysis Project, Quarterly Journal of the Royal Meteorological Society, 137, 1–28, https://doi.org/https://doi.org/10.1002/qj.776.

Dare, R. A. and McBride, J. L.: The threshold sea surface temperature condition for tropical cyclogenesis, Journal of climate, 24, 4570–4576, 2011.

Debreu, L., Vouland, C., and Blayo, E.: AGRIF: Adaptive grid refinement in Fortran, Computers & Geosciences, 34, 8–13, 2008.

Dennison, F., Keeble, J., Morgenstern, O., Zeng, G., Abraham, N. L., and Yang, X.: Improvements to stratospheric chemistry scheme in the UM-UKCA (v10. 7) model: solar cycle and heterogeneous reactions, Geoscientific Model Development, 12, 1227–1239, 2019.

Emanuel, K.: Increasing destructiveness of tropical cyclones over the past 30 years, Nature, 436, 686–688, 2005.

Evans, J. L. and Braun, A.: A climatology of subtropical cyclones in the South Atlantic, Journal of Climate, 25, 7328–7340, 2012.

Fischer, E. M. and Knutti, R.: Robust projections of combined humidity and temperature extremes, Nature Climate Change, 3, 126–130, 2013.

Fricko, O., Havlik, P., Rogelj, J., Klimont, Z., Gusti, M., Johnson, N., Kolp, P., Strubegger, M., Valin, H., Amann, M., et al.: The marker quantification of the Shared Socioeconomic Pathway 2: A middle-of-the-road scenario for the 21st century, Global Environmental Change, 42, 251–267, 2017.

Frölicher, T. L. and Laufkötter, C.: Emerging risks from marine heat waves, Nature communications, 9, 650, 2018.

https://doi.org/10.5194/egusphere-2023-1694
Preprint. Discussion started: 1 August 2023

Fujimori, S., Hasegawa, T., Masui, T., Takahashi, K., Herran, D. S., Dai, H., Hijioka, Y., and Kainuma, M.: SSP3: AIM implementation of Shared Socioeconomic Pathways, Global Environmental Change, 42, 268–283, https://doi.org/https://doi.org/10.1016/j.gloenvcha.2016.06.009, 2017.

Good, P., Sellar, A., Tang, Y., Rumbold, S., Ellis, R., Kelley, D., and Kuhlbrodt, T.: MOHC UKESM1.0-LL model output prepared for CMIP6 ScenarioMIP ssp126, https://doi.org/10.22033/ESGF/CMIP6.6333, 2019a.

Good, P., Sellar, A., Tang, Y., Rumbold, S., Ellis, R., Kelley, D., and Kuhlbrodt, T.: MOHC UKESM1.0-LL model output prepared for CMIP6 ScenarioMIP ssp245, https://doi.org/10.22033/ESGF/CMIP6.6339, 2019b.

Good, P., Sellar, A., Tang, Y., Rumbold, S., Ellis, R., Kelley, D., and Kuhlbrodt, T.: MOHC UKESM1.0-LL model output prepared for CMIP6 ScenarioMIP ssp370, https://doi.org/10.22033/ESGF/CMIP6.6347, 2019c.

Good, P., Sellar, A., Tang, Y., Rumbold, S., Ellis, R., Kelley, D., and Kuhlbrodt, T.: MOHC UKESM1.0-LL model output prepared for CMIP6 ScenarioMIP ssp585, https://doi.org/10.22033/ESGF/CMIP6.6405, 2019d.

Haarsma, R. J., Roberts, M. J., Vidale, P. L., Senior, C. A., Bellucci, A., Bao, Q., Chang, P., Corti, S., Fučkar, N. S., Guemas, V., et al.: High resolution model intercomparison project (HighResMIP v1. 0) for CMIP6, Geoscientific Model Development, 9, 4185–4208, 2016.

Harrington, L., Dean, S., Awatere, S., Rosier, S., Queen, L., Gibson, P., Barnes, C., Zachariah, M., Philip, S., Kew, S., et al.: The role of climate change in extreme rainfall associated with Cyclone Gabrielle over Aotearoa New Zealand's East Coast, 2023.

Hersbach, H., Bell, B., Berrisford, P., Hirahara, S., Horányi, A., Muñoz-Sabater, J., Nicolas, J., Peubey, C., Radu, R., Schepers, D., Simmons, A., Soci, C., Abdalla, S., Abellan, X., Balsamo, G., Bechtold, P., Biavati, G., Bidlot, J., Bonavita, M., De Chiara, G., Dahlgren, P., Dee, D., Diamantakis, M., Dragani, R., Flemming, J., Forbes, R., Fuentes, M., Geer, A., Haimberger, L., Healy, S., Hogan, R. J., Hólm, E., Janisková, M., Keeley, S., Laloyaux, P., Lopez, P., Lupu, C., Radnoti, G., de Rosnay, P., Rozum, I., Vamborg, F., Villaume, S., and Thépaut, J.-N.: The ERA5 global reanalysis, Quarterly Journal of the Royal Meteorological Society, 146, 1999–2049, https://doi.org/https://doi.org/10.1002/qj.3803, 2020.

Hodges, K.: A general method for tracking analysis and its application to meteorological data, Monthly Weather Review, 122, 2573–2586, 1994.

Hodges, K.: Feature tracking on the unit sphere, Monthly Weather Review, 123, 3458–3465, 1995.

Hodges, K.: Adaptive constraints for feature tracking, Monthly Weather Review, 127, 1362–1373, 1999.

Klotzbach, P. J., Oliver, E. C. J., Leeper, R. D., and Schreck, C. J.: The Relationship between the Madden–Julian Oscillation (MJO) and Southeastern New England Snowfall, Monthly Weather Review, 144, 1355 – 1362, https://doi.org/10.1175/MWR-D-15-0434.1, 2016.

Knapp, K. R., Kruk, M. C., Levinson, D. H., Diamond, H. J., and Neumann, C. J.: The international best track archive for climate stewardship (IBTrACS) unifying tropical cyclone data, Bulletin of the American Meteorological Society, 91, 363–376, 2010.

Knutson, T. R., McBride, J. L., Chan, J., Emanuel, K., Holland, G., Landsea, C., Held, I., Kossin, J. P., Srivastava, A., and Sugi, M.: Tropical cyclones and climate change, Nature geoscience, 3, 157–163, 2010.

Kriegler, E., Bauer, N., Popp, A., Humpenöder, F., Leimbach, M., Strefler, J., Baumstark, L., Bodirsky, B. L., Hilaire, J., Klein, D., et al.: Fossil-fueled development (SSP5): An energy and resource intensive scenario for the 21st century, Global environmental change, 42, 297–315, 2017.

Lang, T.: On the uncertainty in modelling tropical relative humidity, Ph.D. thesis, Universität Hamburg Hamburg, 2023.

McTaggart-Cowan, R., Davies, E. L., Fairman, J. G., Galarneau, T. J., and Schultz, D. M.: Revisiting the 26.5° C sea surface temperature threshold for tropical cyclone development, Bulletin of the American Meteorological Society, 96, 1929–1943, 2015.

https://doi.org/10.5194/egusphere-2023-1694
Preprint. Discussion started: 1 August 2023

Meinshausen, M., Nicholls, Z. R., Lewis, J., Gidden, M. J., Vogel, E., Freund, M., Beyerle, U., Gessner, C., Nauels, A., Bauer, N., et al.: The shared socio-economic pathway (SSP) greenhouse gas concentrations and their extensions to 2500, Geoscientific Model Development, 13, 3571–3605, 2020.

Mendelsohn, R., Emanuel, K., Chonabayashi, S., and Bakkensen, L.: The impact of climate change on global tropical cyclone damage, Nature climate change, 2, 205–209, 2012.

Morgenstern, O.: The southern annular mode in 6th coupled model intercomparison project models, Journal of Geophysical Research: Atmospheres, 126, e2020JD034 161, 2021.

Noy, I.: The socio-economics of cyclones, Nature Climate Change, 6, 343–345, 2016.

O'Neill, B. C., Tebaldi, C., Van Vuuren, D. P., Eyring, V., Friedlingstein, P., Hurtt, G., Knutti, R., Kriegler, E., Lamarque, J.-F., Lowe, J., et al.: The scenario model intercomparison project (ScenarioMIP) for CMIP6, Geoscientific Model Development, 9, 3461–3482, 2016.

Peduzzi, P., Chatenoux, B., Dao, H., De Bono, A., Herold, C., Kossin, J., Mouton, F., and Nordbeck, O.: Global trends in tropical cyclone risk, Nature climate change, 2, 289–294, 2012.

Pezza, A. B. and Simmonds, I.: The first South Atlantic hurricane: Unprecedented blocking, low shear and climate change, Geophysical Research Letters, 32, 2005.

Riahi, K., Van Vuuren, D. P., Kriegler, E., Edmonds, J., O'neill, B. C., Fujimori, S., Bauer, N., Calvin, K., Dellink, R., Fricko, O., et al.: The Shared Socioeconomic Pathways and their energy, land use, and greenhouse gas emissions implications: An overview, Global environmental change, 42, 153–168, 2017.

Roberts, M. J., Camp, J., Seddon, J., Vidale, P. L., Hodges, K., Vannière, B., Mecking, J., Haarsma, R., Bellucci, A., Scoccimarro, E., et al.: Projected future changes in tropical cyclones using the CMIP6 HighResMIP multimodel ensemble, Geophysical research letters, 47, e2020GL088 662, 2020a.

Roberts, M. J., Camp, J., Seddon, J., Vidale, P. L., Hodges, K., Vanniere, B., Mecking, J., Haarsma, R., Bellucci, A., Scoccimarro, E., et al.: Impact of model resolution on tropical cyclone simulation using the HighResMIP–PRIMAVERA multimodel ensemble, Journal of Climate, 33, 2557–2583, 2020b.

Sellar, A. A., Jones, C. G., Mulcahy, J. P., Tang, Y., Yool, A., Wiltshire, A., O'connor, F. M., Stringer, M., Hill, R., Palmieri, J., et al.: UKESM1: Description and evaluation of the UK Earth System Model, Journal of Advances in Modeling Earth Systems, 11, 4513–4558, 2019.

Sellar, A. A., Walton, J., Jones, C. G., Wood, R., Abraham, N. L., Andrejczuk, M., Andrews, M. B., Andrews, T., Archibald, A. T., de Mora, L., et al.: Implementation of UK Earth system models for CMIP6, Journal of Advances in Modeling Earth Systems, 12, e2019MS001 946, 2020.

Song, J.-J., Wang, Y., and Wu, L.: Trend discrepancies among three best track data sets of western North Pacific tropical cyclones, Journal of Geophysical Research: Atmospheres, 115, 2010.

Tang, Y., Rumbold, S., Ellis, R., Kelley, D., Mulcahy, J., Sellar, A., Walton, J., and Jones, C.: MOHC UKESM1.0-LL model output prepared for CMIP6 CMIP historical, https://doi.org/10.22033/ESGF/CMIP6.6113, 2019.

Tradowsky, J. S., Bodeker, G. E., Querel, R. R., Builtjes, P. J., and Fischer, J.: Combining data from the distributed GRUAN site Lauder–Invercargill, New Zealand, to provide a site atmospheric state best estimate of temperature, Earth System Science Data, 10, 2195–2211, 2018.

Ullrich, P. A., Zarzycki, C. M., McClenny, E. E., Pinheiro, M. C., Stansfield, A. M., and Reed, K. A.: TempestExtremes v2. 1: A community framework for feature detection, tracking, and analysis in large datasets, Geoscientific Model Development, 14, 5023–5048, 2021.

https://doi.org/10.5194/egusphere-2023-1694
Preprint. Discussion started: 1 August 2023

Van Vuuren, D. P., Stehfest, E., Gernaat, D. E., Doelman, J. C., Van den Berg, M., Harmsen, M., de Boer, H. S., Bouwman, L. F., Daioglou, V., Edelenbosch, O. Y., et al.: Energy, land-use and greenhouse gas emissions trajectories under a green growth paradigm, Global environmental change, 42, 237–250, 2017.

Vecchi, G. A. and Soden, B. J.: Increased tropical Atlantic wind shear in model projections of global warming, Geophysical Research Letters, 34, 2007.

Walsh, J. E., Thoman, R. L., Bhatt, U. S., Bieniek, P. A., Brettschneider, B., Brubaker, M., Danielson, S., Lader, R., Fetterer, F., Holderied, K., et al.: The high latitude marine heat wave of 2016 and its impacts on Alaska, Bull. Am. Meteorol. Soc, 99, S39–S43, 2018.

Walsh, K. J., McBride, J. L., Klotzbach, P. J., Balachandran, S., Camargo, S. J., Holland, G., Knutson, T. R., Kossin, J. P., Lee, T.-c., Sobel, A., et al.: Tropical cyclones and climate change, Wiley Interdisciplinary Reviews: Climate Change, 7, 65–89, 2016.

Williams, J., Behrens, E., Morgenstern, O., Teixeira, J., Varma, V., and Hayek, W.: Regional ocean grid refinement and its effect on simulated atmospheric climate, Authorea Preprints, 2023.

Williams, K., Copsey, D., Blockley, E., Bodas-Salcedo, A., Calvert, D., Comer, R., Davis, P., Graham, T., Hewitt, H., Hill, R., et al.: The Met Office global coupled model 3.0 and 3.1 (GC3. 0 and GC3. 1) configurations, Journal of Advances in Modeling Earth Systems, 10, 357–380, 2018.

Wu, L., Su, H., Fovell, R. G., Wang, B., Shen, J. T., Kahn, B. H., Hristova-Veleva, S. M., Lambrigtsen, B. H., Fetzer, E. J., and Jiang, J. H.: Relationship of environmental relative humidity with North Atlantic tropical cyclone intensity and intensification rate, Geophysical research letters, 39, 2012.

Zhao, A., Brierley, C. M., Jiang, Z., Eyles, R., Oyarzún, D., and Gomez-Dans, J.: Analysing the PMIP4-CMIP6 collection: a workflow and tool (pmip_p2fvar_analyzer v1), Geoscientific Model Development, 15, 2475–2488, 2022.